Molecular Pharmacology Fast Forward. Published on November 5, 2024 as DOI: 10.1124/molpharm.124.000975
This article has not been copyedited and formatted. The final version may differ from this version.

MOLPHARM-AR-2024-000975

Evaluation of allosteric NMDA receptor modulation by GluN2A-selective antagonists using pharmacological equilibrium modeling

James S. Lotti[1], Jaron Jones[1], Jill C. Farnsworth[1], Feng Yi[2], Fabao Zhao[3], Frank S. Menniti[4], Robert A. Volkmann[5], Rasmus P. Clausen[6], and Kasper B. Hansen[1,*]

[1] Center for Structural and Functional Neuroscience, Center for Biomolecular Structure and Dynamics, Division of Biological Sciences, University of Montana, Missoula, MT.

[2] Guangdong-Hong Kong-Macao Greater Bay Area Center for Brain Science and Brain-Inspired Intelligence, Guangdong Basic Research Center of Excellence for Integrated Traditional and Western Medicine for Qingzhi Diseases, Southern Medical University, Guangzhou, China.

[3] Department of Medicinal Chemistry, Key Laboratory of Chemical Biology (Ministry of Education), School of Pharmaceutical Sciences, Shandong University, Jinan, Shandong, China.

[4] MindImmune Therapeutics, Inc., George and Anne Ryan Institute for Neuroscience, University of Rhode Island, Kingston, RI.

[5] BioPharmaWorks, Groton, CT.

[6] Department for Drug Design and Pharmacology, Faculty of Health and Medical Sciences, University of Copenhagen, Copenhagen, Denmark.

* Corresponding author

Molecular Pharmacology Fast Forward. Published on November 5, 2024 as DOI: 10.1124/molpharm.124.000975
This article has not been copyedited and formatted. The final version may differ from this version.

MOLPHARM-AR-2024-000975

Running title: Evaluation of allosteric NMDA receptor modulation

Corresponding author: Kasper B. Hansen, Division of Biological Sciences, University of Montana, 32 Campus Drive, Missoula, MT 59812, USA

Phone: +1 406-243-4820, Email: kasper.hansen@umontana.edu

Number of text pages: 34

Number of figures: 9

Number of tables: 3

Number of references: 92

Words in Abstract: 247

Words in Significance statement: 74

Words in Introduction: 638

Words in Discussion: 1499

Abbreviations:

AICP, (*R*)-2-amino-3-(4-(2-ethylphenyl)-1*H*-indole-2-carboxamido)propanoic acid; CNS, central nervous system; GPCR, G protein-coupled receptor; Me-CCG, (1*S*,2*R*)-2-((S)-amino(carboxy)methyl)-1-methylcyclopropanecarboxylic acid; MTSEA, methanethiosulfonate ethylammonium; NAM, negative allosteric modulator; NMDA, *N*-methyl-D-aspartate; PAM, positive allosteric modulator; UCM-F-8d, (*R*)-2-amino-3-(5-(2-(trifluoromethyl)phenyl)furan-2-carboxamido)propanoic acid.

Molecular Pharmacology Fast Forward. Published on November 5, 2024 as DOI: 10.1124/molpharm.124.000975
This article has not been copyedited and formatted. The final version may differ from this version.

MOLPHARM-AR-2024-000975

Abstract

NMDA-type ionotropic glutamate receptors are critically involved in excitatory neurotransmission and their dysfunction is implicated in many brain disorders. Allosteric modulators with selectivity for specific NMDA receptor subtypes are therefore attractive as therapeutic agents, and sustained drug discovery efforts have resulted in a wide range of new allosteric modulators. However, evaluation of allosteric NMDA receptor modulators is limited by the lack of operational ligand-receptor models to describe modulator binding dissociation constants (K_B) and effects on agonist binding affinity (α) and efficacy (β). Here, we describe a pharmacological equilibrium model that encapsulates activation and modulation of NMDA receptors, and we apply this model to afford deeper understanding of GluN2A-selective negative allosteric modulators (NAMs), TCN-201, MPX-004, and MPX-007. We exploit slow NAM unbinding to examine receptors at hemi-equilibrium when fully occupied by agonists and modulators to demonstrate that TCN-201 display weaker binding and negative modulation of glycine binding affinity (K_B = 42 nM, α = 0.0032) compared to MPX-004 (K_B = 9.3 nM, α = 0.0018) and MPX-007 (K_B = 1.1 nM, α = 0.00053). MPX-004 increases agonist efficacy (β = 1.19), whereas TCN-201 (β = 0.76) and MPX-007 (β = 0.82) reduce agonist efficacy. These values describing allosteric modulation of diheteromeric GluN1/2A receptors with two modulator binding sites are unchanged in triheteromeric GluN1/2A/2B receptors with a single binding site. This evaluation of NMDA receptor modulation reveals differences between ligand analogs that shape their utility as pharmacological tool compounds and facilitates the design of new modulators with therapeutic potential.

Molecular Pharmacology Fast Forward. Published on November 5, 2024 as DOI: 10.1124/molpharm.124.000975
This article has not been copyedited and formatted. The final version may differ from this version.

Significance statement

Detailed understanding of allosteric NMDA receptor modulation requires pharmacological methods to quantify modulator binding affinity and the strengths of modulation of agonist binding and efficacy. We describe a generic ligand-receptor model for allosteric NMDA receptor modulation and use this model for the characterization of GluN2A-selective NAMs. The model enables quantitative evaluation of a broad range of NMDA receptor modulators and provides opportunities to optimize these modulators by embellishing the interpretation of their structure-activity relationships.

Molecular Pharmacology Fast Forward. Published on November 5, 2024 as DOI: 10.1124/molpharm.124.000975
This article has not been copyedited and formatted. The final version may differ from this version.

Introduction

The primary excitatory neurotransmitter in the central nervous system (CNS), glutamate, signals through activation of metabotropic and ionotropic glutamate receptors (Hansen et al., 2021). *N*-methyl-D-aspartate (NMDA) receptors are a class of ionotropic glutamate receptors that are critically involved in neuronal development and many forms of synaptic plasticity relevant to learning and memory (Hansen et al., 2021; Nicoll and Schulman, 2023). Seven different NMDA receptor subunits exist (GluN1, GluN2A-D, and GluN3A-B) that are assembled as heterotetrameric receptor complexes, composed of two obligatory glycine- or D-serine-binding GluN1 subunits and two glutamate-binding GluN2 subunits or two glycine-binding GluN3 subunits (Hansen et al., 2018; Karakas and Furukawa, 2014; Lee et al., 2014; Michalski and Furukawa, 2024). The four GluN2A-D subunits have distinct temporal and spatial expression patterns in the CNS, and the GluN2 subunit identity determines the functional and pharmacological properties of NMDA receptors (Erreger et al., 2007; Monyer et al., 1994; Vicini et al., 1998; Yuan et al., 2009). Diheteromeric NMDA receptors composed of GluN1 and one type of GluN2 subunit (e.g. GluN1/2A) are commonly evaluated in pharmacological studies using heterologous expression systems (e.g. *Xenopus* oocytes and HEK293T cells), albeit triheteromeric NMDA receptor subtypes composed of GluN1 and two different GluN2 subunits (e.g. GluN1/2A/2B) are highly expressed in the adult CNS (reviewed in (Gibb, 2022; Stroebel et al., 2018).

Due to their central role in brain function, NMDA receptors have received considerable attention as therapeutic targets for a wide range of neurological and psychiatric disorders (Hansen et al., 2021; Hanson et al., 2024). In this regard, allosteric NMDA receptor modulators are of

Molecular Pharmacology Fast Forward. Published on November 5, 2024 as DOI: 10.1124/molpharm.124.000975
This article has not been copyedited and formatted. The final version may differ from this version.

particular interest since such agents afford the opportunity to selectively target distinct receptor subtypes to enhance or suppress physiological activity. The rational design of allosteric modulators requires quantitative determination of both modulator binding affinity and efficacy, facilitated by an understanding of the mechanism of action. Commonly, the ligand concentration that elicits half-maximally effective responses (EC_{50}) from cell-surface receptors is used to describe the potency (i.e. potency is $1/EC_{50}$) of agonists or positive allosteric modulators (PAMs). Similarly, the concentration that elicits half-maximally effective inhibition (IC_{50}) is generally used to describe the activity of competitive antagonists, negative allosteric modulators (NAMs), and channel blockers in the case of ion channels. The Hill equation is typically fit to concentration-response data to provide the EC_{50} or IC_{50} values as well as a Hill slope (n_H). However, the parameters derived from the Hill equation do not parse the separable molecular properties that account for functional modulator activity (Colquhoun, 1998; Colquhoun, 2006), including binding affinity at the modulatory binding site and induced changes in agonist binding or efficacy (Ehlert, 2005; Kenakin, 2005). Thus, while EC_{50} or IC_{50} values provide important information that can be used to characterize the functional activity of ligands in biological systems, they alone are not sufficient to enable the quantitative comparisons between ligands required to efficiently optimize their functional activity (Colquhoun, 1998; Colquhoun, 2006). Here, we derive a pharmacological equilibrium model that describes agonist binding and activation as well as allosteric modulation of NMDA receptors. This model defines receptor open probability as a function of agonist and modulator concentrations using five parameters, namely agonist and modulator dissociation constants (K_A and K_B, respectively), agonist efficacy (E), allosteric binding interaction constant (α), and allosteric efficacy interaction constant (β). Thus, we describe modulator efficacy according to the strength by which modulator binding changes

Molecular Pharmacology Fast Forward. Published on November 5, 2024 as DOI: 10.1124/molpharm.124.000975
This article has not been copyedited and formatted. The final version may differ from this version.

agonist binding affinity (α) and/or agonist efficacy (β) (Gibb, 2022; Kenakin, 2017). Using this model, we provide new insights to inhibition of both diheteromeric and triheteromeric GluN2A-containing NMDA receptors by the GluN2A-selective NAMs, TCN-201, MPX-004, and MPX-007 (Bettini et al., 2010; Hansen et al., 2012; Volkmann et al., 2016; Yi et al., 2016). Our analysis provides a deeper understanding of allosteric modulation by GluN2A-selective antagonists, predicts their activity under physiological conditions, and facilitates the development of novel modulators with improved therapeutic potential.

Molecular Pharmacology Fast Forward. Published on November 5, 2024 as DOI: 10.1124/molpharm.124.000975
This article has not been copyedited and formatted. The final version may differ from this version.

Materials and Methods

DNA constructs and ligands

The cDNAs for rat GluN1-1a (GenBank accession numbers U11418 and U08261; hereafter GluN1), rat GluN2A (D13211), and rat GluN2B (U11419) were inserted into pCI-neo vectors for expression in *Xenopus* laevis oocytes and HEK293T cells. For expression in *Xenopus* oocytes, the rat GluN2B cDNA was modified to remove a T7 RNA polymerase termination site located in the C-terminal domain as previously described (Hansen et al., 2014). For estimation of open probability, the A652C mutation was introduced into the GluN1 subunit. For expression of triheteromeric NMDA receptors, previously described DNA constructs were used, in which the C-terminal domain for GluN2A was swapped into GluN2B ($GluN2B_{2A}$) and peptide tags composed of $GABA_B$ receptor heterodimeric coiled-coil motifs (C1 and C2) and endoplasmic reticulum retention signal were spliced onto the C-terminus of GluN2A and $GluN2B_{2A}$ (herafter referred to as $GluN2A_{C1}$ and $GluN2B_{C2}$) (Hansen et al., 2014; Yi et al., 2017). For visualization of transfected HEK293T cells and titration of NMDA receptor expression levels, EGFP was inserted between the CMV promoter of the pCI-neo vector and the open reading frame (ORF) of GluN1 (i.e. GluN1 and EGFP are expressed as individual proteins), and 0-3 start codons encoding small upstream ORFs were placed between the open reading frames of EGFP and GluN1 as previously described (Yi et al., 2018).

TCN-201 and MPX-004 were purchased from Hello Bio (Princeton, NJ) and Alomone Labs (Jerusalem, Israel), respectively. MPX-007 (Volkmann et al., 2016), UCM-F-8d (compound 8d from (Zhao et al., 2022), and Me-CCG (compound 4b from (Risgaard et al., 2013) were synthesized as previously described. Purities of the tested compounds were determined by

Molecular Pharmacology Fast Forward. Published on November 5, 2024 as DOI: 10.1124/molpharm.124.000975
This article has not been copyedited and formatted. The final version may differ from this version.

analytical HPLC to be >95%. Stock solutions for glutamate and glycine were prepared at 10 mM and 100 mM, respectively, in recording solutions. Stock solutions of all other ligands were prepared at 10-100 mM in DMSO. The concentration of DMSO was kept constant throughout recordings and never exceeded a concentration of 0.3 %.

Two-electrode voltage-clamp recordings

For expression in *Xenopus laevis* oocytes, the cDNAs were linearized using restriction enzymes to produce templates for *in vitro* cRNA synthesis (mMessage mMachine, Thermo Fisher Scientific, Waltham, MA). *Xenopus* oocytes purchased from Xenopus1 (Dexter, MI) were maintained and prepared for cDNA injection as previously described (Hansen et al., 2013). Oocytes were injected with *in vitro* synthesized cRNAs and stored at 17°C or 19°C for diheteromeric or triheteromeric NMDA receptors, respectively (Hansen et al., 2014; Yi et al., 2017). Oocytes were maintained in modified Barth's solution containing (in mM) 88 NaCl, 2.4 $NaHCO_3$, 1 KCl, 0.33 $Ca(NO3)_2$, 0.41 $CaCl_2$, 0.82 $MgSO_4$, and 10 HEPES (pH 7.5 with NaOH) supplemented with 1 IU/ml penicillin, 1 µg/ml streptomycin (Gibco, Thermo Fisher Scientific, Waltham, MA), and 50 µg/ml gentamycin (Fisher Scientific, Hampton, NH). For experiments with diheteromeric NMDA receptors, the cRNAs encoding GluN1 and GluN2 were combined at variable ratios and diluted with RNase-free water to achieve a desirable expression level. For experiments with triheteromeric NMDA receptors, the cRNAs encoding GluN1, $GluN2A_{C1}$, and $GluN2B_{C2}$ were diluted with RNase-free water at a 1:1:1 ratio. Each oocyte was injected with a total volume of 50 nL cRNA.

Two-electrode voltage clamp recordings were performed 2-4 days after injection at room temperature (23°C). The extracellular recording solution contained (in mM) 90 NaCl, 1 KCl, 0.5

Molecular Pharmacology Fast Forward. Published on November 5, 2024 as DOI: 10.1124/molpharm.124.000975
This article has not been copyedited and formatted. The final version may differ from this version.

BaCl2, 0.01 EDTA, and 10 HEPES (pH 7.4 with NaOH). Solution exchange was computer-controlled through two 8-modular valve positioners (Hamilton Company, Reno, NV). Voltage and current electrodes were pulled using a vertical puller (PC-10, Narishige, Amityville, NY) and filled with 3.0 M KCl. Current responses were recorded at a holding potential of -40 mV using a two-electrode voltage-clamp amplifier (OC-725C; Warner Instruments, Hamden, CT). Measurements were low-pass filtered at 20 Hz (Alligator Technologies, Charlottesville, VA) before they were passed to a digitizer (PCIe-6321, National Instruments, Austin, TX) for data acquisition. On the day of recordings, oocytes were injected with 30-50 nL of 50 mM BAPTA to prevent activity-dependent increases in the amplitude of the response (Williams, 1993). Solutions of methanethiosulfonate ethylammonium (MTSEA) were prepared fresh at a concentration of 0.2 mM and used for recordings within 30 min. For experiments with triheteromeric receptors, the fraction of current response from "escaped" receptors compared to the total current response was always determined on the day of the experiment as previously described, and experiments were only performed if the "escape" current response was <10% of the total current response (Yi et al., 2017).

Whole-cell voltage-clamp recordings

HEK293T cells were plated in 24-well plates approximately 48 hours prior to recording and cultured in Dulbecco's modified Eagle's medium (DMEM) with GlutaMax-I and sodium pyruvate supplemented with 10% fetal bovine serum, 10 U/mL penicillin, and 10 µg/mL streptomycin (Gibco, Thermo Fisher Scientific, Waltham, MA). The HEK293T cells are from previously published studies (Elmasri et al., 2022; Rouzbeh et al., 2023) and were not authenticated experimentally or tested for mycoplasma contamination for this study.

Molecular Pharmacology Fast Forward. Published on November 5, 2024 as DOI: 10.1124/molpharm.124.000975
This article has not been copyedited and formatted. The final version may differ from this version.

Transfections were performed the day before recording using the calcium phosphate precipitation method (Chen and Okayama, 1987) with 0.5 μg of total DNA per 24-well as previously described (Hansen et al., 2013). For experiments with diheteromeric receptors, DNA constructs encoding GluN1 and GluN2 were transfected at a 1:1 ratio. For experiments with triheteromeric receptors, DNA constructs encoding GluN1 and the two distinct GluN2 subunits were transfected at a 1:1:1 ratio (GluN1/GluN2$_{C1}$/GluN2B$_{C2}$). To prevent NMDA receptor-mediated cytotoxicity, the media was supplemented with 200 μM 7-chlorokynurenic acid (7CKA) and 200 μM D,L-2-amino-5-phosphonovalerate (AP5) following transfection. On the day of recording, the transfected cells were mechanically triturated in DMEM using repetitive pipetting, before they were replated onto poly-D-lysine coated (0.1 mg/mL) glass coverslips in cell culture medium and given at least 3 hours to re-adhere. Whole-cell patch-clamp recordings were performed at room temperature (21–23 °C) using an Axopatch 200B amplifier (Molecular Devices, San Jose, CA) and a holding potential of –60 mV. The signal was low-pass filtered at 8 kHz (8-pole, –3 dB Bessel, Frequency Devices, Ottawa, IL), digitized at 20 kHz using Digidata 1322A (Molecular Devices), and recorded with pCLAMP software (Molecular Devices). Thin-wall glass micropipettes (BF150-110-10, Sutter Instrument Company, Novato, CA) were pulled using a horizontal puller (P-1000, Sutter Instrument Company, Novato, CA) to produce recording electrodes with a tip resistance of 2-4MΩ. Recording electrodes were filled with internal solution containing (in mM) 110 D-gluconate, 110 CsOH, 30 CsCl, 4 NaCl, 0.5 $CaCl_2$, 2 $MgCl_2$, 5 BAPTA, 2 NaATP, 0.3 NaGTP, and 5 HEPES (pH 7.35 with CsOH). The extracellular recording solution consisted of (in mM) 150 NaCl, 3 KCl, 0.5 $CaCl_2$, 0.01 EDTA, and 10 HEPES (pH 7.4 with NaOH). Solutions were applied to the cells by gravity-driven perfusion through an 8-channel stepper motor (Warner Instruments, Hamden, CT) with 10-90% open-tip solution exchange times less than 2 ms. Cells

Molecular Pharmacology Fast Forward. Published on November 5, 2024 as DOI: 10.1124/molpharm.124.000975
This article has not been copyedited and formatted. The final version may differ from this version.

with access resistance >10 MΩ or >30% drift in response amplitudes during recordings were excluded from data analysis.

Data analysis

Maximal open probability (P_{open}) was estimated from the maximal current response to agonist in the absence ($I_{agonist}$) and presence of MTSEA (I_{MTSEA}), where MTSEA covalently reacts with GluN1-A652C to lock the channel in an open conformation with $P_{open} \approx 1$ (Jones et al., 2002; Yuan et al., 2005). To adjust for changes in single channel conductance following MTSEA exposure, maximal P_{open} was calculated using the following equation (Yuan et al., 2005):

$$P_{open}^{\infty} = \frac{\gamma_{MTSEA}}{\gamma_{agonist}} \times \frac{I_{agonist}}{I_{MTSEA}}$$

The values of $\gamma_{MTSEA}/\gamma_{agonist}$ were 0.66 for $GluN1_{A652C}/2A$ and $GluN1_{A652C}/2A_{C1}/2B_{C2}$ and 0.69 for $GluN1_{A652C}/2B$ receptors (Yuan et al., 2005; Yuan et al., 2009).

Concentration–response data were analyzed with GraphPad Prism (GraphPad Software, La Jolla, CA). Agonist concentration-response data for individual oocytes were fit by the Hill equation:

$$I = I_{min} + \frac{I_{max} - I_{min}}{1 + 10^{((\log[A] - \log EC_{50}) \times n_H)}}$$

I_{max} and I_{min} are the fitted maximum and minimum responses to agonist, n_H is the Hill slope, [A] is the agonist concentration, and EC_{50} is the effective agonist concentration that produces half-maximum response. For agonists, the fitted I_{min} is typically negligible and close to zero. Unless otherwise stated, data points from individual oocytes were normalized to I_{max} and I_{min} and averaged for graphical representation.

To determine agonist binding affinity K_a, agonist efficacy E, modulator binding affinity K_b,

Molecular Pharmacology Fast Forward. Published on November 5, 2024 as DOI: 10.1124/molpharm.124.000975
This article has not been copyedited and formatted. The final version may differ from this version.

allosteric binding constant α, and allosteric efficacy constant β, we derived the following equation according to the law of mass action and the equilibrium model shown in Figure 1 (see Supplemental Information for the derivation):

$$P_{open} = \frac{Ex^2(1+\alpha\beta y)^2}{(1+y)^2 + 2x(1+y+\alpha y+\alpha y^2) + x^2(1+\alpha y)^2 + Ex^2(1+\alpha\beta y)^2} \quad \textbf{(Equation 1)}$$

Here, $x = [A]K_a$ and $y = [B]K_b$, where [A] and [B] are agonist and modulator concentrations, respectively. At supersaturating concentrations of agonist ($[A] \to \infty$ and therefore also $x \to \infty$) and modulator ($[B] \to \infty$ and $y \to \infty$), the limit of Equation 1 describes maximal P_{open} with modulatory binding sites fully occupied:

$$P_{open}^{\infty} = \frac{\beta^2 E}{1+\beta^2 E} \quad \textbf{(Equation 2)}$$

If agonist efficacy E and maximal P_{open} in the presence of NAM are known, then the allosteric efficacy constant β can be calculated:

$$\beta = \sqrt{\frac{P_{open}^{\infty}}{E(1-P_{open}^{\infty})}} \quad \textbf{(Equation 3)}$$

In the absence of modulator (y = 0), Equation 1 reduces to the following:

$$P_{open} = \frac{Ex^2}{1+2x+x^2+Ex^2} \quad \textbf{(Equation 4)}$$

At supersaturating concentrations of agonist ($[A] \to \infty$ and $x \to \infty$) the limit of Equation 3 describes maximal P_{open} in the absence of modulator:

$$P_{open}^{\infty} = \frac{E}{1+E} \quad \textbf{(Equation 5)}$$

Molecular Pharmacology Fast Forward. Published on November 5, 2024 as DOI: 10.1124/molpharm.124.000975
This article has not been copyedited and formatted. The final version may differ from this version.

$$E = \frac{P_{open}^{\infty}}{1 - P_{open}^{\infty}} \qquad \textbf{(Equation 6)}$$

When agonist efficacy E is known, the agonist binding affinity K_a (or agonist dissociation constant $K_A = 1/K_a$) can be determined by fitting a normalized version of Equation 3 to agonist concentration-response data:

$$I = I_{min} + (I_{max} + I_{min}) \times \frac{1 + E}{E} \times \frac{Ex^2}{1 + 2x + x^2 + Ex^2} \qquad \textbf{(Equation 7)}$$

When agonist binding affinity K_a, agonist efficacy E, allosteric binding constant α, and allosteric efficacy constant β are known, the modulator binding affinity K_b (or modulator dissociation constant $K_B = 1/K_b$) can be determined by fitting a normalized version of Equation 1 using global non-linear regression to agonist concentration-response data in the absence and presence of different modulator concentrations:

$$I = I_{min} + (I_{max} + I_{min}) \times \frac{1 + \beta^2 E}{\beta^2 E} \times \frac{Ex^2(1 + \alpha\beta y)^2}{(1 + y)^2 + 2x(1 + y + \alpha y + \alpha y^2) + x^2(1 + \alpha y)^2 + Ex^2(1 + \alpha\beta y)^2} \qquad \textbf{(Equation 8)}$$

When agonist binding affinity K_a, agonist efficacy E, and allosteric efficacy constant β are known at supersaturating concentrations of modulator ($[B] \to \infty$ and $y \to \infty$), the allosteric binding constant α can be determined by fitting agonist concentration-response data in the presence of a saturating modulator concentration to the following equation:

$$I = I_{min} + (I_{max} + I_{min}) \times \frac{1 + \beta^2 E}{\beta^2 E} \times \frac{\alpha^2\beta^2 Ex^2}{1 + 2\alpha x + \alpha^2 x^2 + \alpha^2\beta^2 Ex^2} \qquad \textbf{(Equation 9)}$$

Assuming one binding site for GluN2A-selective NAMs in triheteromeric GluN1/2A/2B receptors, Equations 2, 3 and 9 are changed to the following:

Molecular Pharmacology Fast Forward. Published on November 5, 2024 as DOI: 10.1124/molpharm.124.000975
This article has not been copyedited and formatted. The final version may differ from this version.

$$P_{open}^{\infty} = \frac{\beta E}{1 + \beta E} \quad \textbf{(Equation 10)}$$

$$\beta = \frac{P_{open}^{\infty}}{E(1 - P_{open}^{\infty})} \quad \textbf{(Equation 11)}$$

$$I = I_{min} + (I_{max} + I_{min}) \times \frac{1 + \beta E}{\beta E} \times \frac{\alpha \beta E x^2}{1 + \alpha x + x + \alpha x^2 + \alpha \beta E x^2} \quad \textbf{(Equation 12)}$$

Statistical analysis

Data are expressed as mean ± SD unless otherwise stated. Experiments were not designed with a predetermined number of replicates. Statistical analyses were performed as described in figure and table legends. Experiments in this exploratory study were designed to test biological hypotheses and calculated p-values should be interpreted as descriptive. Significance for all tests was set at $p < 0.05$.

Molecular Pharmacology Fast Forward. Published on November 5, 2024 as DOI: 10.1124/molpharm.124.000975
This article has not been copyedited and formatted. The final version may differ from this version.

Results

The majority of neuronal NMDA receptors are comprised of two GluN1 and two GluN2 subunits, arranged as a dimer of GluN1-GluN2 dimers, that form a central ion channel pore (Hansen et al., 2021). TCN-201, MPX-004 and MPX-007 are NAMs of diheteromeric and triheteromeric GluN2A-containing NMDA receptors, and the GluN2A selectivity derives from the NAM binding site in the subunit interface between the GluN1-GluN2A agonist binding domains. We developed a pharmacological equilibrium model to determine differences among the GluN2A-selective NAMs in terms of their binding affinity as well as their effects on agonist affinity and efficacy, that is, the molecular characteristics that contribute to the differentiable pharmacology of these allosteric modulators.

Assumptions and definitions of the pharmacological equilibrium model

The pharmacological equilibrium model describes allosteric modulation in terms of three parameters, namely, modulator binding affinity K_b, allosteric binding constant α, and allosteric efficacy constant β (Fig. 1). This model also describes the effects of allosteric modulation on agonist binding affinity K_a (i.e. the association equilibrium constant) and agonist efficacy E. Since NMDA receptors require full agonist occupancy at both coagonist binding sites (e.g. glutamate and glycine) for activation (Benveniste and Mayer, 1991; Clements and Westbrook, 1991), the model considers the binding of one coagonist (e.g. glycine) and assumes full occupancy by the other coagonist (e.g. glutamate). The model assumes that the two agonist binding sites for each coagonist are equivalent and independent (Benveniste and Mayer, 1991; Clements and Westbrook, 1991), that the allosteric modulator has two equivalent and independent binding sites, consistent with a single binding site in each GluN1-GluN2 subunit

Molecular Pharmacology Fast Forward. Published on November 5, 2024 as DOI: 10.1124/molpharm.124.000975
This article has not been copyedited and formatted. The final version may differ from this version.

dimer in the tetrameric NMDA receptor subunit complex (Hackos et al., 2016; Karakas et al., 2011; Romero-Hernandez et al., 2016; Yi et al., 2016). Agonist efficacy E represents the transition of the fully agonist-bound receptor to the open state from an ensemble of closed states (Auerbach and Zhou, 2005; Banke and Traynelis, 2003; Erreger et al., 2005; Gibb et al., 2018; Iacobucci and Popescu, 2017; Schorge et al., 2005) and it is assumed that receptor desensitization, if any, occurs only from the fully agonist-bound conformation (Fig. 1). Based on the model, we derived an equation using the law of mass action to describe NMDA receptor open probability at equilibrium as a function of agonist and modulator concentrations (Equation 1, see also Supplemental Information for the derivation). The equation can be fitted to experimental data to quantify the parameters that underlie agonist and modulator activity.

Binding affinity and efficacy for glutamate and glycine site agonists

Determination of agonist efficacy E requires that receptor responses are described in terms of channel open probability (P_{open}). According to Equation 5, agonist efficacy E can be calculated from the maximal P_{open} in response to the agonist. Previous studies have employed a modified soluble cysteine accessibility method to estimate maximal P_{open} for GluN1/2A NMDA receptors (Yuan et al., 2005; Yuan et al., 2009). In this approach, a cysteine residue is inserted in the NMDA receptor ion channel at position Ala652 in the GluN1 subunit, and maximal agonist responses with and without cysteine modification by MTSEA are measured. MTSEA covalently reacts with GluN1-A652C in the open channel pore, locking the channel in an open conformation with $P_{open} \approx 1$, thereby enabling calculation of maximal P_{open} from the ratio of responses before and after MTSEA modification (Yuan et al., 2005) (see Materials and Methods). Using this approach, we estimated maximal P_{open} for five different coagonist combinations at GluN1-

Molecular Pharmacology Fast Forward. Published on November 5, 2024 as DOI: 10.1124/molpharm.124.000975
This article has not been copyedited and formatted. The final version may differ from this version.

A652C/2A receptors (Fig. 2A-C, Table 1). Because all four agonist binding sites, i.e. both the two glycine binding sites and the two glutamate binding sites, must be occupied for channel opening (Benveniste and Mayer, 1991; Clements and Westbrook, 1991), the maximal P_{open} and agonist efficacy are specific to each coagonist pair. To substantiate the approach to estimate maximal P_{open}, we selected agonists that are expected to have a range of binding affinities and efficacies. AICP is a GluN1 agonist with an extraordinary high potency, but a maximum response similar to glycine (Jessen et al., 2017), while UCM-F-8d is a GluN1 agonist with a high potency and yet a much lower maximal response compared to glycine (Zhao et al., 2022). Maximal P_{open} values were 0.39 for glutamate/glycine, 0.36 for glutamate/AICP, and 0.044 for glutamate/UCM-F-8d (Table 1). Thus, AICP is nearly a full agonist and UCM-F-8d is a partial agonist compared to glycine, consistent with functional characterization in previous studies (Jessen et al., 2017; Zhao et al., 2022). Me-CCG is a partial GluN2 agonists with a higher potency compared to glutamate (Risgaard et al., 2013). Maximal P_{open} values were 0.29 for NMDA/glycine and 0.29 for Me-CCG/glycine (Table 1), demonstrating that NMDA and Me-CCG are both partial agonists compared to glutamate as previously shown (Erreger et al., 2007; Hansen et al., 2008; Risgaard et al., 2013). Agonist efficacy E values calculated from maximal P_{open} using Equation 4 were 0.66 for glutamate/glycine, 0.57 for glutamate/AICP, 0.046 for glutamate/UCM-F-8d, 0.41 for NMDA/glycine, and 0.42 for Me-CCG/glycine (Table 1). Maximal P_{open} for glutamate/glycine estimated here using the modified soluble cysteine accessibility method are similar to previously published values determined using single-channel recordings from GluN1/2A receptors (Schorge et al., 2005; Yuan et al., 2009).

With agonist efficacy E known, it is possible to obtain agonist binding affinity K_a by fitting Equation 7 to normalized concentration-response data at GluN1/2A receptors. In the presence of

Molecular Pharmacology Fast Forward. Published on November 5, 2024 as DOI: 10.1124/molpharm.124.000975
This article has not been copyedited and formatted. The final version may differ from this version.

a saturating glutamate concentration (300 μM), the binding dissociation constants K_A were 0.66 μM for glycine, 0.041 μM for AICP, and 0.033 μM for UCM-F-8d (Fig. 2D-F, Table 1). Fitting the same data to the Hill equation gave EC_{50} values of 1.03 μM for glycine, 0.064 μM for AICP, and 0.082 μM for UCM-F-8d (Table 1). In the presence of a saturating glycine concentration (100 μM), the binding dissociation constants K_A were 2.2 μM for glutamate, 50 μM for NMDA, and 0.11 μM for Me-CCG (Fig. 2D-F, Table 1). From fitting the Hill equation, the corresponding EC_{50} values were 3.4 μM for glutamate, 88 μM for NMDA, and 0.21 μM for Me-CCG (Table 1).

In summary, AICP and UCM-F-8d display considerable variation in agonist efficacy at the glycine site of GluN1/2A receptors, but have similar binding affinities that are 16- to 20-fold higher than glycine. NMDA and Me-CCG are both partial glutamate site agonists with similar agonist efficacies, but binding affinities compared to glutamate are 23-fold lower for NMDA and 20-fold higher for Me-CCG. This quantitative determination of agonist activities at GluN1/2A receptors enables the evaluation of allosteric modulators to determine their effects on agonist binding affinity and efficacy.

Challenges related to characterization of GluN2A-selective negative allosteric modulation

GluN2A-selective NAMs, TCN-201, MPX-004, and MPX-007, bind the heterodimer interface formed between agonist binding domains of GluN1 and GluN2A subunits (Yi et al., 2016). It has been previously demonstrated that binding of these GluN2A-selective NAMs inhibits NMDA receptors by reducing glycine potency, and glycine binding reciprocally reduces NAM binding affinity (Edman et al., 2012; Hansen et al., 2012; Yi et al., 2016). Thus, similar to competitive antagonists, the inhibition by GluN2A-selective NAMs can be surmounted by high concentrations of glycine. However, unlike competitive antagonists, GluN2A-selective NAMs

Molecular Pharmacology Fast Forward. Published on November 5, 2024 as DOI: 10.1124/molpharm.124.000975
This article has not been copyedited and formatted. The final version may differ from this version.

and agonists can simultaneously bind the NMDA receptor. Using a simplified version of the equilibrium model shown in Figure 1, in which modulation is described by a single agonist binding step, a single modulator binding step, and no modulation of agonist efficacy (Christopoulos and Kenakin, 2002; Ehlert, 1988), the binding dissociation constant K_B and allosteric binding interaction constant α for TCN-210 were previously estimated to be approximately 27-45 nM and 0.003-0.007, respectively (Hansen et al., 2012; Yi et al., 2016). While K_B and α have not been estimated for MPX-004 and MPX-007, previous concentration-inhibition data obtained using electrophysiological measurements indicate that the three GluN2A-selective NAMs display similar potencies in the presence of 3 μM glycine, but that more glycine is required to surmount inhibition by MPX-004 and MPX-007 compared to TCN-201 (Yi et al., 2016). However, in a separate study, MPX-007 was reported to be 10-fold more potent than TCN-201 using measurements of intracellular calcium levels (Volkmann et al., 2016). It remains unknown whether the seemingly stronger inhibition by MPX-004 and MPX-007 compared to TCN-201 is mediated by improvements in binding affinity and/or allosteric interactions. Furthermore, variation among the GluN2A-selective NAMs in their ability to change agonist efficacy may also contribute to the observed differences in potency (Volkmann et al., 2016; Yi et al., 2016).

Binding affinity and allosteric constants (K_b, α, and β) for TCN-201, MPX-004, and MPX-007 can, in theory, be determined by fitting Equation 8 with fixed agonist binding affinity K_a and efficacy E to a series of glycine concentration-response data in the absence and presence of increasing modulator concentrations. To minimize ambiguity in the fitting process, concentration-response data at low NAM concentrations should be included to accurately determine the binding dissociation constant K_B. Furthermore. high NAM concentrations are

Molecular Pharmacology Fast Forward. Published on November 5, 2024 as DOI: 10.1124/molpharm.124.000975
This article has not been copyedited and formatted. The final version may differ from this version.

required to obtain sufficient shifts in the concentration-response data to determine allosteric constants (α and β). However, poor solubility of TCN-201, MPX-004, and MPX-007 prevents their reliable use at concentrations higher than 5 μM, 10 μM, and 30 μM in two-electrode voltage-clamp recordings (Volkmann et al., 2016), which may not reveal maximal modulation of agonist binding affinity or efficacy. Furthermore, as demonstrated in Figure 3, MPX-004 and MPX-007 display remarkably slow onset and offset of inhibition, in particular at lower concentrations, which makes equilibrium difficult to attain in a reasonable time. These results highlight practical challenges that commonly occur in functional assays of receptor pharmacology related to insufficient time to reach agonist/modulator/receptor equilibrium and the omission of saturating ligand-receptor conditions due to poor ligand solubility (Charlton and Vauquelin, 2010; Kenakin, 2017).

Determination of allosteric efficacy constant β at hemi-equilibrium

In the absence of equilibrium conditions and with proper corrections to the ligand-receptor model, measurements at hemi-equilibrium (i.e. before full agonist/modulator/receptor equilibrium is observed; (Paton and Rang, 1966) can represent a useful compromise for pharmacological evaluation of ligands with slow unbinding kinetics (Charlton and Vauquelin, 2010; Kenakin et al., 2006; Riddy et al., 2015). The time constants for offset of inhibition at GluN1/2A receptors by TCN-201 are slow, depending on glycine and NAM concentrations (35-50 s for 3-10 μM TCN-201 inhibition in 10 μM glycine) (Hansen et al., 2012), and the kinetics of MPX-004 and MPX-007 are presumably slower (Fig. 3). We took advantage of the slow unbinding to determine the allosteric efficacy constant β at hemi-equilibrium when GluN1/2A receptors are fully bound by NAM and maximally activated by glycine.

Molecular Pharmacology Fast Forward. Published on November 5, 2024 as DOI: 10.1124/molpharm.124.000975
This article has not been copyedited and formatted. The final version may differ from this version.

We performed whole-cell patch-clamp experiments with HEK293T cells expressing GluN1/2A receptors to enable fast solution exchange (see Materials and Methods). Responses to a supersaturating concentration of glycine (30 mM) were measured before and after equilibration with a NAM concentration predicted to fully occupy the modulatory binding sites in the absence of agonist (3 μM TCN-201, 10 μM MPX-004, 10 μM MPX-007). Using this approach, maximal glycine responses were measured at hemi-equilibrium before substantial NAM unbinding can occur (Fig. 4). There was no discernable unbinding of MPX-004 and MPX-007 during the 2 second response activated by 30 mM glycine, whereas some unbinding was observed for TCN-201 with a time constant of 230 ± 100 ms (N = 6) from a mono-exponential decay fit (Fig. 4B). Thus, response amplitudes were measured at the initial peak after fast glycine application when the receptors are fully bound by NAM and maximally activated by glycine.

Responses measured before NAM exposure are activated with agonist efficacy E = 0.66 (Fig. 2, Table 1). According to the model (Fig. 1), responses measured from receptors with bound NAM are activated with agonist efficacy β^2E. Because maximal P_{open} in the absence of NAM is known, maximal P_{open} in the presence of NAM can be estimated from the ratio of responses before and after NAM exposure and the allosteric efficacy constant β can be calculated using Equation 3. TCN-201 and MPX-007 inhibited the maximal glycine response to 71% ± 9% (N = 10) and 80% ± 13% (n = 8), respectively, compared to control (Fig. 4C), corresponding to allosteric efficacy constants of β = 0.76 for TCN-201 and β = 0.82 for MPX-007 (Table 2). By contrast, MPX-004 increased maximal glycine responses to 124% ± 10% (N = 10) compared to control (Fig. 4C), corresponding to an allosteric efficacy constant of β = 1.19 (Table 2). Thus, while all three GluN2A NAMs inhibit NMDA receptors by reducing glycine potency, they display variation in their allosteric efficacy interactions with TCN-201 and MPX-007 reducing

Molecular Pharmacology Fast Forward. Published on November 5, 2024 as DOI: 10.1124/molpharm.124.000975
This article has not been copyedited and formatted. The final version may differ from this version.

agonist efficacy and MPX-004 increasing agonist efficacy.

Modulation of glutamate potency by GluN2A-selective NAMs

To corroborate the β values determined at hemi-equilibrium, we isolated the effects of the GluN2A-selective NAMs on receptor efficacy apart from interactions with glycine by using a receptor mutant that requires only glutamate for activation. We introduced a disulfide bond in GluN1 (GluN1-N499C+Q686C, hereafter GluN1-CC) that restricts the agonist binding domain in a closed conformation that mimics the glycine bound state to enable receptor activation by glutamate alone (Dai and Zhou, 2016; Kussius and Popescu, 2010; Sun et al., 2017; Yi et al., 2016). In GluN1-CC/2A receptors, the GluN2A-selective NAMs are therefore unable to inhibit by reducing glycine potency, and NAM-induced changes in glutamate-activated response amplitudes are due to allosteric efficacy interactions described by β.

Glutamate concentration-response data were measured for GluN1-CC/2A in the absence and presence of NAM (5 μM TCN-201, 10 μM MPX-004, 10 μM MPX-007). Glutamate EC_{50} values were not significantly different between vehicle (EC_{50} = 2.11 μM) and in the presence of TCN-201 (EC_{50} = 2.53 μM) (Fig. 5, Table 3). However, MPX-004 and MPX-007 significantly decreased glutamate EC_{50} to 1.08 μM and 1.30 μM, respectively, compared to vehicle (Fig. 5, Table 3). Responses were normalized to a maximal glutamate response at the beginning of the recording before vehicle or NAM exposure (Fig. 5B). The fitted maximal glutamate response from the concentration-response data was not significantly different between vehicle and in the presence of TCN-201 (91% in 0.05% DMSO versus 88% in TCN-201) or MPX-007 (88% in 0.1% DMSO versus 87% in MPX-007). By contrast, MPX-004 significantly increased the fitted maximal glutamate response (88% in 0.1% DMSO versus 104% in MPX-004) (Fig. 5, Table 3).

Molecular Pharmacology Fast Forward. Published on November 5, 2024 as DOI: 10.1124/molpharm.124.000975
This article has not been copyedited and formatted. The final version may differ from this version.

The vehicle control reveals that the response amplitudes are slightly reduced over the duration of the recordings. These results should be interpreted with the caveat that the GluN2A-selective NAMs may exhibit incomplete or no binding to GluN1-CC/2A, since the crosslinked GluN1 agonist binding conformation represents the low affinity NAM binding site (e.g. as illustrated in Figure 1) (Yi et al., 2016). This caveat notwithstanding, the results are consistent with β values determined at hemi-equilibrium that indicate the NAMs have distinct allosteric effects on receptor activation. These results also are consistent with a previous conclusion that the GluN2A-selective NAMs do not inhibit NMDA receptors by reducing glutamate potency (Bettini et al., 2010; Hansen et al., 2012; Yi et al., 2016).

Determination of allosteric binding constant α at hemi-equilibrium

Like the determination of the allosteric efficacy constant β (Fig. 4, Table 2), the slow NAM unbinding enabled evaluation of the allosteric binding constant α at hemi-equilibrium using whole-cell patch-clamp with fast solution exchange (i.e. solution exchange times less than 2 ms). Responses from HEK293T cells expressing GluN1/2A receptors to a range of glycine concentrations were measured after equilibration with vehicle (0.1% DMSO) or a high NAM concentration (3 μM TCN-201, 10 μM MPX-004, and 10 μM MPX-007). Thus, glycine concentration-response data can be generated at hemi-equilibrium before NAM unbinding occurs, and glycine binding affinity corresponds to K_a in vehicle and αK_a when the receptors a fully occupied by GluN2A NAM. For experiments with MPX-004 and MPX-007, the receptors were exposed to glycine for 1000 ms, which did not result in any discernable NAM unbinding. For experiments with TCN-201, the glycine exposure was limited to 15 ms to minimize NAM unbinding. To determine K_a (or $1/K_A$) under these experimental conditions, Equation 7 with

Molecular Pharmacology Fast Forward. Published on November 5, 2024 as DOI: 10.1124/molpharm.124.000975
This article has not been copyedited and formatted. The final version may differ from this version.

agonist efficacy E fixed to 0.66 was fitted to concentration-response data in vehicle (0.05% DMSO for TCN-201, and 0.1% DMSO for MPX-004 and MPX-007). Values for glycine K_A (i.e. dissociation binding constants) were 0.93 μM (0.81 - 1.07 μM 95% CI, N = 9, Table 1) following 1000 ms glycine exposures (i.e. steady-state responses) and 5.6 μM (4.0 - 7.8 μM 95% CI, N = 7) following 15 ms exposures (i.e. peak responses) (Fig. 6). These differences in K_A values may reflect differences in agonist affinity and efficacy for steady-state responses (1000 ms) and peak responses (15 ms). To determine the allosteric binding constant α, Equation 9 with fixed K_a, E, and β was fitted to concentration response data in the presence of GluN2A-selective NAMs. The α values were 0.0032 for TCN-201, 0.0018 for MPX-004, and 0.00053 for MPX-007 (Fig. 6, Table 2). Thus, MPX-007 exhibits stronger allosteric modulation of glycine binding affinity compared to TCN-201 and MPX-004 (Table 2).

Determination of modulator binding dissociation constant K_B

To determine modulator binding affinity K_b, we generated glycine concentration-response data at GluN1/2A receptors using two-electrode voltage-clamp recordings. Equilibrium responses were reached following long (2.5-5 min) glycine exposures in the absence of NAMs and in the presence of low to high TCN-201 concentration, whereas equilibrium could only be reached in the presence of high MPX-004 and MPX-007 concentrations (Fig. 7). For MPX-004 and MPX-007, equilibrium could not be reached at low NAM concentrations close to the modulator binding dissociation constant K_B (Fig. 3). The modulator binding affinity K_b was determined by fitting Equation 8 with fixed K_a, E, α, and β to the glycine concentration-response data using global nonlinear regression. The best fit K_B values (i.e. binding dissociation constants) were 42 nM for TCN-201, 9.3 nM for MPX-004, and 1.1 nM for MPX-007 (Fig. 7, Table 2). To investigate the

Molecular Pharmacology Fast Forward. Published on November 5, 2024 as DOI: 10.1124/molpharm.124.000975
This article has not been copyedited and formatted. The final version may differ from this version.

uncertainty in the global nonlinear regression due to the lack low concentrations of MPX-004 and MPX-007, we calculated the sum of squared errors (SSE) of the fit of Equation 8 with fixed K_a, E, α, and β to the glycine concentration-response data as a function of the binding dissociation constant K_B. These calculations reveal a single global SSE minimum for each of the GluN2A-selective NAMs (Fig. 7C). Thus, this approach to determine K_B values is relatively robust. However, plots of calculated SSE for the fit of Equation 8 with K_b and α or β as free parameters illustrate that global nonlinear regression has the potential to yield ambiguous results if multiple parameters are fitted simultaneously using only a few intermediate to high NAM concentrations. (Supplemental Fig. S1). That is, shifts in glycine concentration-response data mediated by a few intermediate to high NAM concentrations are influenced by the modulator binding affinity K_b as well as by the strength in allosteric interactions (i.e. α and β). Notwithstanding these considerations, this approach identifies differences in binding affinity between the GluN2A-selective NAMs.

Inhibition of triheteromeric GluN1/2A/2B receptors by GluN2A-selective NAMs

Triheteromeric receptors composed of two GluN1 and two different GluN2 subunits are the predominant NMDA receptor subtypes in the central nervous system, with principal neurons in most regions of the adult forebrain mainly expressing GluN1/2A/2B receptors (Gray et al., 2011; Rauner and Kohr, 2011; Yi et al., 2019). The therapeutic potential of GluN2A-selective antagonists and their utility as pharmacological tool compounds therefore depend on their activity on triheteromeric GluN1/2A/2B receptors. To quantify the activity of TCN-201, MPX-004, and MPX-007 at GluN1/2A/2B receptors using the same approach as described for GluN1/2A, we assumed that the NAMs only have one binding site in GluN1/2A/2B receptors with a binding

Molecular Pharmacology Fast Forward. Published on November 5, 2024 as DOI: 10.1124/molpharm.124.000975
This article has not been copyedited and formatted. The final version may differ from this version.

affinity K_b identical to that determined for GluN1/2A receptors, and that glycine binding affinity is identical for the two GluN1 subunits in GluN1/2A/2B receptors.

We used the modified soluble cysteine accessibility method and two-electrode voltage-clamp electrophysiology to determine maximal P_{open} values of 0.15 for triheteromeric GluN1-A652C/2A/2B and 0.026 for diheteromeric GluN1-A652C/2B receptors activated by glutamate/glycine (Fig. 8A, Table 1). These maximal P_{open} values correspond to agonist efficacies E of 0.17 for GluN1-A652C/2A/2B and 0.026 for GluN1-A652C/2B receptors (Table 1). Using these agonist efficacy E values, we determined agonist binding dissociation constants K_A from glycine concentration-response data measured using whole-cell patch-clamp recordings (Figure 8). The glycine binding dissociation constant K_A was 0.48 μM for GluN1/2A/2B and 0.27 μM for GluN1/2B receptors (Table 1). These values are lower (i.e. higher binding affinity K_a) compared to GluN1/2A (0.93 μM).

Values for α and β were determined at hemi-equilibrium using the same approach as described for GluN1/2A, except Equation 12 was fitted to the concentration-response data in the presence of NAM (Fig. 8B-C). Values of the allosteric efficacy constant β were found to be 0.75 for TCN-201, 1.28 for MPX-004, and 0.84 for MPX-007 (Fig. 8B, Table 2). These β values determined at triheteromeric GluN1/2A/2B receptors were not significantly different from their counterparts at diheteromeric NMDA receptors (Table 2). At triheteromeric GluN1/2A/2B receptors, values of the allosteric binding constant α were found to be 0.0068 for TCN-201, 0.0021 for MPX-004, and 0.00074 for MPX-007, all of which are not significantly different from the values determined in diheteromeric GluN1/2A receptors (Fig. 8C,D, Table 2). These results are consistent with minimal allosteric effects mediated by the GluN2B subunit in triheteromeric NMDA receptors and a dominant allosteric influence of the GluN2A subunit as previously

described (Hansen et al., 2014; Lu et al., 2017; Sun et al., 2017).

In summary, the evaluation of GluN2A NAM activity at triheteromeric GluN1/2A/2B and diheteromeric GluN1/2A receptors demonstrates that allosteric constants α and β remain unchanged irrespectively of the number of NAM binding sites, consistent with identical and independent binding sites at the GluN1-GluN2A subunit interface (Yi et al., 2016), and a dominant influence of the GluN2A subunit in triheteromeric GluN1/2A/2B receptors (Hansen et al., 2014; Sun et al., 2017).

Simulations of allosteric modulation by GluN2A-selective antagonists

To illustrate modulation of GluN1/2A receptors at equilibrium, we simulated glycine concentration-response data in the absence and presence of GluN2A-selective NAMs using the experimentally determined parameters listed in Tables 1 and 2 (Fig. 9A). These simulations highlight the benefit of determining allosteric constants α and β at hemi-equilibrium with receptors saturated by NAM, since full modulation at equilibrium would require NAM concentrations above or close to the solubility limits (8 µM, 16 µM, and 68 µM for TCN-201, MPX-004, and MPX-007, respectively; (Volkmann et al., 2016). While it is theoretically possible to evaluate MPX-004 and MPX-007 at a near-saturating concentration, the prolonged time required to reach agonist/modulator/receptor equilibrium further imposes practical limitations to the functional assays (Fig. 3). Simulations of NAM concentration-inhibition data in the presence of increasing glycine suggest that complete inhibition of diheteromeric GluN1/2A receptors can be achieved by 5 µM TCN-201 in the presence of up to 3-10 µM glycine, which is within physiologically relevant glycine and D-serine levels (0.5-10 µM; (Bae et al., 2021; Bergeron et al., 1998; Billups and Attwell, 2003; Ishiwata et al., 2015) (Fig. 9B). More robust inhibition of

Molecular Pharmacology Fast Forward. Published on November 5, 2024 as DOI: 10.1124/molpharm.124.000975
This article has not been copyedited and formatted. The final version may differ from this version.

GluN1/2A receptors is achieved by 10 μM MPX-004 and 10 μM MPX-007 that display complete inhibition in the presence of up to 30 μM or 100 μM glycine, respectively (Fig. 9B). At triheteromeric GluN1/2A/2B receptors, complete inhibition by 5 μM TCN-201 is surmounted already at ~1-3 μM glycine, whereas 10 μM MPX-004 or 10 μM MPX-007 can produce full inhibition up to ~3-10 μM or ~30 μM glycine, respectively (Fig. 9C). Thus, these simulations using experimentally determined binding affinities and allosteric constants demonstrate that a soluble concentration of MPX-007 produces more robust inhibition of physiologically relevant GluN2A-containing NMDA receptors compared to soluble concentrations of TCN-201 and MPX-004. These results also suggest that soluble concentrations of MPX-004 and MPX-007 can produce close to complete inhibition of GluN2A-containing NMDA receptors at physiologically relevant concentrations of glycine or D-serine (0.5-10 μM; (Bae et al., 2021; Bergeron et al., 1998; Billups and Attwell, 2003; Ishiwata et al., 2015).

Molecular Pharmacology Fast Forward. Published on November 5, 2024 as DOI: 10.1124/molpharm.124.000975
This article has not been copyedited and formatted. The final version may differ from this version.

Discussion

NMDA receptors are activated by agonists that increase the probability of the channel entering and staying in the open state. The NMDA receptor complex also harbors binding sites through which physiological and xenobiotic ligands may further allosterically modulate channel activity. Given the essential roles of NMDA receptors in excitatory neurotransmission and synaptic plasticity, pharmacological modulation of their activity has therapeutic potential across the spectrum of CNS disorders. The development of new NMDA receptor-targeted therapeutics may be facilitated by detailed investigation of modulator characteristics, including affinity for allosteric sites and effects resulting from binding these sites. With this in mind, we describe a pharmacological equilibrium model for allosteric modulation of NMDA receptors that enables determinations of modulator binding dissociation constants (K_B) and effects on agonist binding affinity (α) and efficacy (β).

Using the model, we determined binding affinities and efficacies for glutamate site agonists (glutamate, NMDA, and Me-CCG) and glycine site agonists (glycine, AICP, and UCM-F-8d) with diverse chemical structures and variation in binding affinity and efficacy, presumably by engaging in distinct binding pocket interactions to stabilize different agonist binding domain conformations (Dai and Zhou, 2015; Erreger et al., 2005; Hansen et al., 2005; Hansen et al., 2013; Inanobe et al., 2005; Vance et al., 2011). The lack of apparent correlation between agonist affinity and efficacy supports this interpretation, since such correlation would be expected for highly similar NMDA receptor agonist structures (Hansen et al., 2013; Kalbaugh et al., 2004; Nayak et al., 2019). In nicotinic acetylcholine receptors, the correlation between efficacy and affinity, which is determined by the output/input energy ratio of the receptor, has been termed

Molecular Pharmacology Fast Forward. Published on November 5, 2024 as DOI: 10.1124/molpharm.124.000975
This article has not been copyedited and formatted. The final version may differ from this version.

agonist efficiency (Auerbach, 2016; Nayak et al., 2019). Furthermore, the agonist efficiency is conserved among structurally similar receptor agonists, but efficiencies vary among different structural classes of agonists (Auerbach, 2016; Indurthi and Auerbach, 2021; Indurthi and Auerbach, 2023; Nayak et al., 2019). Binding affinities and efficacies determined in this study enable similar analysis for NMDA receptor agonists. Thus, glycine, AICP, and UCM-F-8d have agonist efficiencies of 36%, 31%, and 27%, respectively (calculated as described in Indurthi and Auerbach (2021) with $E_0 = 1.68*10^{-7}$ from Nayak et al. (2019)). Thus, glycine displays higher efficiency (low affinity, high efficacy), AICP has intermediate efficiency (high affinity, high efficacy), and UCM-F-8d has lower efficiency (high affinity, low efficacy). This analysis can be readily expanded to include NMDA receptor agonists with previously reported EC_{50} values and relative maximal responses (Chen et al., 2008; Erreger et al., 2007), which can be converted to agonist binding dissociation constants (K_A) and efficacies (E) using the following equations:

$$\mathrm{E} = \frac{\mathrm{R_{max}}}{\frac{1+\mathrm{E_G}}{\mathrm{E_G}} - \mathrm{R_{max}}}, \qquad \mathrm{EC_{50}} = \frac{\mathrm{K_A}(1+\sqrt{E+2})}{\mathrm{E}+1}$$

R_{max} is the maximal response relative to glycine/glutamate and E_G is the agonist efficacy for glycine/glutamate (e.g. as reported in Table 1). Thus, the ability to discern agonist binding affinity and efficacy facilitates nuanced investigations of mechanisms that correlate agonist binding and receptor gating, and improve interpretation of functional effects caused by receptor mutations (Colquhoun, 1998; Erreger et al., 2007; Hansen et al., 2005; Laube et al., 2004).

The model was applied to investigate modulation by GluN2A-selective NAMs, TCN-201, MPX-004, and MPX-007, that bind the interface between the agonist binding domains of GluN1 and GluN2A subunits (Hansen et al., 2012; Yi et al., 2016). These GluN2A-selective NAMs exemplify limitations of IC_{50} values as the single parameter for comparing allosteric modulators,

Molecular Pharmacology Fast Forward. Published on November 5, 2024 as DOI: 10.1124/molpharm.124.000975
This article has not been copyedited and formatted. The final version may differ from this version.

since the three NAMs display similar potencies in physiological glycine concentrations but differ in the glycine concentration required to surmount their inhibition (Volkmann et al., 2016; Yi et al., 2016). Here, using the model, we show that these NAMs differ both in their binding affinity and in their effects on agonist affinity and efficacy. For GluN1/2A receptors fully bound by glycine, the NAM binding dissociation constants are shifted to K_B/α, corresponding to 13 μM for TCN-201, 5.2 μM for MPX-004, and 2.1 μM for MPX-007. Conversely, glycine potency is shifted from 1.05 μM in the absence of NAM to 380 μM at GluN1/2A receptors fully bound by TCN-201, 510 μM for MPX-004, 2200 μM for MPX-007 (K_A changes to K_A/α and E changes to β^2E). This quantitative evaluation is consistent with descriptions from previous studies (Volkmann et al., 2016; Yi et al., 2016) and suggest that higher binding affinities and more negative interactions with glycine binding mediate stronger modulation by MPX-004 and MPX-007 compared to TCN-201 at physiologically-relevant glycine concentrations. Despite similarities in the chemical structures of the MPX analogs, TCN-201 has an allosteric binding constant (α) comparable to MPX-004, while the allosteric efficacy constant (β) of TCN-201 is similar to MPX-007. The determination of which components of the chemical structures that mediate allosteric modulation of agonist binding affinity (α) and/or efficacy (β) would require similar comparisons for additional TCN and MPX analogs. Thus, the determination of K_B, α, and β embellishes the interpretation of structure-activity relationships and enables rational design of novel modulators with enhanced properties.

We also evaluated the activity of the GluN2A-selective NAMs at triheteromeric GluN1/2A/2B receptors. We demonstrate that K_B, α, and β values are conserved between diheteromeric GluN1/2A and triheteromeric GluN1/2A/2B receptors irrespective of the number for NAM binding sites. This result is consistent with previous studies suggesting that the

Molecular Pharmacology Fast Forward. Published on November 5, 2024 as DOI: 10.1124/molpharm.124.000975
This article has not been copyedited and formatted. The final version may differ from this version.

GluN2A subunit imparts a dominant influence on functional properties related to agonist binding in triheteromeric GluN1/2A/2B receptors (Hansen et al., 2014; Lu et al., 2017; Sun et al., 2017). That is, the GluN2A-selective NAMs inhibit GluN1/2A and GluN1/2A/2B receptors with similar binding affinity and efficacy (α and β), and differences in concentration-inhibition data are mediated by the distinct agonist activity and number of NAM binding sites in two receptor subtypes. Further studies are required to determine if this feature of GluN2A-selective NAMs is also observed for other modulator binding sites, other classes of allosteric modulators (e.g. GluN2A-selective PAMs; (Hackos et al., 2016) or other GluN2A-containing receptor subtypes (e.g. GluN1/2A/2C; (Bhattacharya et al., 2018). While the notion of identical and independent modulator binding at subunit interfaces seems at odds with allosteric models derived in other receptor systems (e.g. GPCRs and pentameric receptors) where binding sites between subunits are not independent (Changeux, 2013; Changeux and Christopoulos, 2016), this observation aligns nicely with previous studies revealing independent subunit-specific conformational changes that influence pre-gating steps in NMDA receptors (Auerbach and Zhou, 2005; Banke and Traynelis, 2003; Erreger et al., 2005; Gibb et al., 2018; Schorge et al., 2005).

Poor solubility of the GluN2A-selective NAMs and slow time to reach equilibrium represented challenges by limiting the range of concentrations that could be studied. To overcome this limitation, we conducted some experiments under “hemi-equilibrium” conditions. The term “hemi-equilibrium” was originally used to describe the condition that occurs when the agonist response, measured in the presence of a pre-equilibrated antagonist concentration, is mediated by the equilibrium interaction between agonist and receptor without any concomitant perturbation in the pre-existing antagonist equilibrium (Paton and Rang, 1966). We exploited the slow unbinding kinetics of the GluN2A-selective NAMs to achieve hemi-equilibrium conditions

Molecular Pharmacology Fast Forward. Published on November 5, 2024 as DOI: 10.1124/molpharm.124.000975
This article has not been copyedited and formatted. The final version may differ from this version.

by measuring the rapid response to agonist before any appreciable changes in NAM-receptor occupancy could occur. This "hemi-equilibrium" approach also mitigates issues related to poor modulator solubility that would otherwise prevent equilibrium measurements in saturated agonist/modulator/receptor conditions required to appreciate full modulation of agonist potency and efficacy (Charlton and Vauquelin, 2010; Christopoulos et al., 1999; Kenakin et al., 2006).

In recent years, there has been a remarkable expansion in the synthetic pharmacology of NMDA receptors, resulting in a diverse range of new allosteric modulators (Burnell et al., 2019; Geoffroy et al., 2022; Hansen et al., 2021; Hanson et al., 2024; Wu et al., 2023). However, the study of NMDA receptors has lagged behind other surface receptors, such as GPCRs, for which operational ligand-receptor models have been widely applied to quantify allosteric modulation (Kenakin, 2017). With the exception of the GluN2A-selective NAMs, new NMDA receptor modulators have not been evaluated in the context of operational ligand-receptor models to explicitly determine K_B, α, and β. For example, binding of GluN2A-selective PAMs (e.g. GNE-6901 and GNE-8324) increases glutamate potency ($\alpha > 1$) and may also increase agonist efficacy ($\beta > 1$) (Hackos and Hanson, 2017; Hackos et al., 2016). GluN2B-selective antagonists (e.g. ifenprodil) have been suggested to increase agonist potency ($\alpha > 1$), while primarily reducing agonist efficacy ($\beta < 1$) (Amico-Ruvio et al., 2012; Bhatt et al., 2013; Kew et al., 1996; Mott et al., 1998). Some GluN2C/D-selective antagonists (e.g. QNZ46 and DQP-1105) require glutamate for binding (suggesting $\alpha > 1$), but also reduce agonist efficacy ($\beta < 1$) (Acker et al., 2011; Hansen and Traynelis, 2011). The binding affinities for these and other NMDA receptor modulators are unknown due to the problem of discerning binding (K_B) and effect (α and β) from EC_{50} or IC_{50} values. The pharmacological equilibrium model can be readily applied to these other classes of allosteric NMDA receptor modulators. Thus, quantitative understanding of the

Molecular Pharmacology Fast Forward. Published on November 5, 2024 as DOI: 10.1124/molpharm.124.000975
This article has not been copyedited and formatted. The final version may differ from this version.

parameters that govern potency and functional effects of allosteric modulation can improve the utility of pharmacological tool compounds and enable more detailed interpretation of structure-activity relationships that facilitate structure-based design of novel modulators with improved therapeutic potential.

Acknowledgements

We thank Gina C. Bullard for excellent technical assistance.

Data Availability Statement

The authors declare that all the data supporting the findings of this study are available within the paper and its Supplemental Data.

Authorship Contributions

Participated in research design: Lotti, Farnsworth, Yi, Hansen.

Conducted experiments: Lotti, Farnsworth, Yi.

Performed data analysis: Lotti, Jones, Farnsworth, Yi, Hansen.

Wrote or contributed to the writing of the manuscript: Lotti, Jones, Farnsworth, Yi, Zhao, Menniti, Volkmann, Clausen, Hansen.

References

Acker TM, Yuan H, Hansen KB, Vance KM, Ogden KK, Jensen HS, Burger PB, Mullasseril P, Snyder JP, Liotta DC and Traynelis SF (2011) Mechanism for noncompetitive inhibition by novel GluN2C/D N-methyl-D-aspartate receptor subunit-selective modulators. *Mol Pharmacol* **80**(5): 782-795.

Amico-Ruvio SA, Paganelli MA, Myers JM and Popescu GK (2012) Ifenprodil effects on GluN2B-containing glutamate receptors. *Mol Pharmacol* **82**(6): 1074-1081.

Auerbach A (2016) Dose-Response Analysis When There Is a Correlation between Affinity and Efficacy. *Mol Pharmacol* **89**(2): 297-302.

Auerbach A and Zhou Y (2005) Gating reaction mechanisms for NMDA receptor channels. *J Neurosci* **25**(35): 7914-7923.

Bae M, Roh JD, Kim Y, Kim SS, Han HM, Yang E, Kang H, Lee S, Kim JY, Kang R, Jung H, Yoo T, Kim H, Kim D, Oh H, Han S, Kim D, Han J, Bae YC, Kim H, Ahn S, Chan AM, Lee D, Kim JW and Kim E (2021) SLC6A20 transporter: a novel regulator of brain glycine homeostasis and NMDAR function. *EMBO Mol Med* **13**(2): e12632.

Banke TG and Traynelis SF (2003) Activation of NR1/NR2B NMDA receptors. *Nat Neurosci* **6**(2): 144-152.

Benveniste M and Mayer ML (1991) Kinetic analysis of antagonist action at N-methyl-D-aspartic acid receptors. Two binding sites each for glutamate and glycine. *Biophys J* **59**(3): 560-573.

Bergeron R, Meyer TM, Coyle JT and Greene RW (1998) Modulation of N-methyl-D-aspartate receptor function by glycine transport. *Proc Natl Acad Sci U S A* **95**(26): 15730-15734.

Bettini E, Sava A, Griffante C, Carignani C, Buson A, Capelli AM, Negri M, Andreetta F, Senar-Sancho SA, Guiral L and Cardullo F (2010) Identification and characterization of novel NMDA receptor antagonists selective for NR2A- over NR2B-containing receptors. *J Pharmacol Exp Ther* **335**(3): 636-644.

Bhatt JM, Prakash A, Suryavanshi PS and Dravid SM (2013) Effect of ifenprodil on GluN1/GluN2B N-methyl-D-aspartate receptor gating. *Mol Pharmacol* **83**(1): 9-21.

Bhattacharya S, Khatri A, Swanger SA, DiRaddo JO, Yi F, Hansen KB, Yuan H and Traynelis SF (2018) Triheteromeric GluN1/GluN2A/GluN2C NMDARs with Unique Single-Channel Properties Are the Dominant Receptor Population in Cerebellar Granule Cells. *Neuron* **99**(2): 315-328 e315.

Billups D and Attwell D (2003) Active release of glycine or D-serine saturates the glycine site of NMDA receptors at the cerebellar mossy fibre to granule cell synapse. *Eur J Neurosci* **18**(11): 2975-2980.

Burnell ES, Irvine M, Fang G, Sapkota K, Jane DE and Monaghan DT (2019) Positive and Negative Allosteric Modulators of N-Methyl-d-aspartate (NMDA) Receptors: Structure-Activity Relationships and Mechanisms of Action. *J Med Chem* **62**(1): 3-23.

Changeux JP (2013) 50 years of allosteric interactions: the twists and turns of the models. *Nat Rev Mol Cell Biol* **14**(12): 819-829.

Changeux JP and Christopoulos A (2016) Allosteric Modulation as a Unifying Mechanism for Receptor Function and Regulation. *Cell* **166**(5): 1084-1102.

Charlton SJ and Vauquelin G (2010) Elusive equilibrium: the challenge of interpreting receptor pharmacology using calcium assays. *Br J Pharmacol* **161**(6): 1250-1265.

Chen C and Okayama H (1987) High-efficiency transformation of mammalian cells by plasmid DNA. *Mol Cell Biol* **7**(8): 2745-2752.

Chen PE, Geballe MT, Katz E, Erreger K, Livesey MR, O'Toole KK, Le P, Lee CJ, Snyder JP, Traynelis SF and Wyllie DJ (2008) Modulation of glycine potency in rat recombinant NMDA receptors containing chimeric NR2A/2D subunits expressed in Xenopus laevis oocytes. *J Physiol* **586**(1): 227-245.

Christopoulos A (1998) Assessing the distribution of parameters in models of ligand-receptor interaction: to log or not to log. *Trends Pharmacol Sci* **19**(9): 351-357.

Christopoulos A and Kenakin T (2002) G protein-coupled receptor allosterism and complexing. *Pharmacol Rev* **54**(2): 323-374.

Christopoulos A, Parsons AM, Lew MJ and El-Fakahany EE (1999) The assessment of antagonist potency under conditions of transient response kinetics. *Eur J Pharmacol* **382**(3): 217-227.

Clements JD and Westbrook GL (1991) Activation kinetics reveal the number of glutamate and glycine binding sites on the N-methyl-D-aspartate receptor. *Neuron* **7**(4): 605-613.

Colquhoun D (1998) Binding, gating, affinity and efficacy: the interpretation of structure-activity relationships for agonists and of the effects of mutating receptors. *Br J Pharmacol* **125**(5): 924-947.

Colquhoun D (2006) The quantitative analysis of drug-receptor interactions: a short history. *Trends Pharmacol Sci* **27**(3): 149-157.

Dai J and Zhou HX (2015) Reduced curvature of ligand-binding domain free-energy surface underlies partial agonism at NMDA receptors. *Structure* **23**(1): 228-236.

Dai J and Zhou HX (2016) Semiclosed Conformations of the Ligand-Binding Domains of NMDA Receptors during Stationary Gating. *Biophys J* **111**(7): 1418-1428.

Edman S, McKay S, Macdonald LJ, Samadi M, Livesey MR, Hardingham GE and Wyllie DJ (2012) TCN 201 selectively blocks GluN2A-containing NMDARs in a GluN1 co-agonist dependent but non-competitive manner. *Neuropharmacology* **63**(3): 441-449.

Ehlert FJ (1988) Estimation of the affinities of allosteric ligands using radioligand binding and pharmacological null methods. *Mol Pharmacol* **33**(2): 187-194.

Ehlert FJ (2005) Analysis of allosterism in functional assays. *J Pharmacol Exp Ther* **315**(2): 740-754.

Elmasri M, Lotti JS, Aziz W, Steele OG, Karachaliou E, Sakimura K, Hansen KB and Penn AC (2022) Synaptic Dysfunction by Mutations in GRIN2B: Influence of Triheteromeric NMDA Receptors on Gain-of-Function and Loss-of-Function Mutant Classification. *Brain Sci* **12**(6).

Erreger K, Geballe MT, Dravid SM, Snyder JP, Wyllie DJ and Traynelis SF (2005) Mechanism of partial agonism at NMDA receptors for a conformationally restricted glutamate analog. *J Neurosci* **25**(34): 7858-7866.

Erreger K, Geballe MT, Kristensen A, Chen PE, Hansen KB, Lee CJ, Yuan H, Le P, Lyuboslavsky PN, Micale N, Jorgensen L, Clausen RP, Wyllie DJ, Snyder JP and Traynelis SF (2007) Subunit-specific agonist activity at NR2A-, NR2B-, NR2C-, and NR2D-containing N-methyl-D-aspartate glutamate receptors. *Mol Pharmacol* **72**(4): 907-920.

Geoffroy C, Paoletti P and Mony L (2022) Positive allosteric modulation of NMDA receptors: mechanisms, physiological impact and therapeutic potential. *J Physiol* **600**(2): 233-259.

Gibb AJ (2022) Allosteric antagonist action at triheteromeric NMDA receptors. *Neuropharmacology* **202**: 108861.

Gibb AJ, Ogden KK, McDaniel MJ, Vance KM, Kell SA, Butch C, Burger P, Liotta DC and Traynelis SF (2018) A structurally derived model of subunit-dependent NMDA receptor function. *J Physiol* **596**(17): 4057-4089.

Gray JA, Shi Y, Usui H, During MJ, Sakimura K and Nicoll RA (2011) Distinct modes of AMPA receptor suppression at developing synapses by GluN2A and GluN2B: single-cell NMDA receptor subunit deletion in vivo. *Neuron* **71**(6): 1085-1101.

Hackos DH and Hanson JE (2017) Diverse modes of NMDA receptor positive allosteric modulation: Mechanisms and consequences. *Neuropharmacology* **112**(Pt A): 34-45.

Hackos DH, Lupardus PJ, Grand T, Chen Y, Wang TM, Reynen P, Gustafson A, Wallweber HJ, Volgraf M, Sellers BD, Schwarz JB, Paoletti P, Sheng M, Zhou Q and Hanson JE (2016) Positive Allosteric Modulators of GluN2A-Containing NMDARs with Distinct Modes of Action and Impacts on Circuit Function. *Neuron* **89**(5): 983-999.

Hansen KB, Brauner-Osborne H and Egebjerg J (2008) Pharmacological characterization of

ligands at recombinant NMDA receptor subtypes by electrophysiological recordings and intracellular calcium measurements. *Comb Chem High Throughput Screen* **11**(4): 304-315.

Hansen KB, Clausen RP, Bjerrum EJ, Bechmann C, Greenwood JR, Christensen C, Kristensen JL, Egebjerg J and Brauner-Osborne H (2005) Tweaking agonist efficacy at N-methyl-D-aspartate receptors by site-directed mutagenesis. *Mol Pharmacol* **68**(6): 1510-1523.

Hansen KB, Ogden KK and Traynelis SF (2012) Subunit-selective allosteric inhibition of glycine binding to NMDA receptors. *J Neurosci* **32**(18): 6197-6208.

Hansen KB, Ogden KK, Yuan H and Traynelis SF (2014) Distinct functional and pharmacological properties of Triheteromeric GluN1/GluN2A/GluN2B NMDA receptors. *Neuron* **81**(5): 1084-1096.

Hansen KB, Tajima N, Risgaard R, Perszyk RE, Jorgensen L, Vance KM, Ogden KK, Clausen RP, Furukawa H and Traynelis SF (2013) Structural determinants of agonist efficacy at the glutamate binding site of N-methyl-D-aspartate receptors. *Mol Pharmacol* **84**(1): 114-127.

Hansen KB and Traynelis SF (2011) Structural and mechanistic determinants of a novel site for noncompetitive inhibition of GluN2D-containing NMDA receptors. *J Neurosci* **31**(10): 3650-3661.

Hansen KB, Wollmuth LP, Bowie D, Furukawa H, Menniti FS, Sobolevsky AI, Swanson GT, Swanger SA, Greger IH, Nakagawa T, McBain CJ, Jayaraman V, Low CM, Dell'Acqua ML, Diamond JS, Camp CR, Perszyk RE, Yuan H and Traynelis SF (2021) Structure, Function, and Pharmacology of Glutamate Receptor Ion Channels. *Pharmacol Rev* **73**(4): 298-487.

Hansen KB, Yi F, Perszyk RE, Furukawa H, Wollmuth LP, Gibb AJ and Traynelis SF (2018) Structure, function, and allosteric modulation of NMDA receptors. *J Gen Physiol* **150**(8): 1081-1105.

Hanson JE, Yuan H, Perszyk RE, Banke TG, Xing H, Tsai MC, Menniti FS and Traynelis SF (2024) Therapeutic potential of N-methyl-D-aspartate receptor modulators in psychiatry. *Neuropsychopharmacology* **49**(1): 51-66.

Iacobucci GJ and Popescu GK (2017) NMDA receptors: linking physiological output to biophysical operation. *Nat Rev Neurosci* **18**(4): 236-249.

Inanobe A, Furukawa H and Gouaux E (2005) Mechanism of partial agonist action at the NR1 subunit of NMDA receptors. *Neuron* **47**(1): 71-84.

Indurthi DC and Auerbach A (2021) Agonist efficiency from concentration-response curves: Structural implications and applications. *Biophys J* **120**(9): 1800-1813.

Indurthi DC and Auerbach A (2023) Agonist efficiency links binding and gating in a nicotinic receptor. *eLife* **12**.

Ishiwata S, Umino A, Balu DT, Coyle JT and Nishikawa T (2015) Neuronal serine racemase regulates extracellular D-serine levels in the adult mouse hippocampus. *J Neural Transm (Vienna)* **122**(8): 1099-1103.

Jessen M, Frederiksen K, Yi F, Clausen RP, Hansen KB, Brauner-Osborne H, Kilburn P and Damholt A (2017) Identification of AICP as a GluN2C-Selective N-Methyl-d-Aspartate Receptor Superagonist at the GluN1 Glycine Site. *Mol Pharmacol* **92**(2): 151-161.

Jones KS, VanDongen HM and VanDongen AM (2002) The NMDA receptor M3 segment is a conserved transduction element coupling ligand binding to channel opening. *J Neurosci* **22**(6): 2044-2053.

Kalbaugh TL, VanDongen HM and VanDongen AM (2004) Ligand-binding residues integrate affinity and efficacy in the NMDA receptor. *Mol Pharmacol* **66**(2): 209-219.

Karakas E and Furukawa H (2014) Crystal structure of a heterotetrameric NMDA receptor ion channel. *Science* **344**(6187): 992-997.

Karakas E, Simorowski N and Furukawa H (2011) Subunit arrangement and phenylethanolamine binding in GluN1/GluN2B NMDA receptors. *Nature* **475**(7355): 249-253.

Kenakin T (2005) New concepts in drug discovery: collateral efficacy and permissive antagonism. *Nat Rev Drug Discov* **4**(11): 919-927.

Kenakin T (2017) The Quantitative Characterization of Functional Allosteric Effects. *Curr Protoc Pharmacol* **76**: 9 22 21-29 22 10.

Kenakin T, Jenkinson S and Watson C (2006) Determining the potency and molecular mechanism of action of insurmountable antagonists. *J Pharmacol Exp Ther* **319**(2): 710-723.

Kew JN, Trube G and Kemp JA (1996) A novel mechanism of activity-dependent NMDA receptor antagonism describes the effect of ifenprodil in rat cultured cortical neurones. *J Physiol* **497 (Pt 3)**(Pt 3): 761-772.

Kussius CL and Popescu GK (2010) NMDA receptors with locked glutamate-binding clefts open with high efficacy. *J Neurosci* **30**(37): 12474-12479.

Laube B, Schemm R and Betz H (2004) Molecular determinants of ligand discrimination in the glutamate-binding pocket of the NMDA receptor. *Neuropharmacology* **47**(7): 994-1007.

Lee CH, Lu W, Michel JC, Goehring A, Du J, Song X and Gouaux E (2014) NMDA receptor structures reveal subunit arrangement and pore architecture. *Nature* **511**(7508): 191-197.

Lu W, Du J, Goehring A and Gouaux E (2017) Cryo-EM structures of the triheteromeric NMDA receptor and its allosteric modulation. *Science* **355**(6331).

Michalski K and Furukawa H (2024) Structure and function of GluN1-3A NMDA receptor excitatory glycine receptor channel. *Sci Adv* **10**(15): eadl5952.

Monyer H, Burnashev N, Laurie DJ, Sakmann B and Seeburg PH (1994) Developmental and regional expression in the rat brain and functional properties of four NMDA receptors. *Neuron* **12**(3): 529-540.

Mott DD, Doherty JJ, Zhang S, Washburn MS, Fendley MJ, Lyuboslavsky P, Traynelis SF and Dingledine R (1998) Phenylethanolamines inhibit NMDA receptors by enhancing proton inhibition. *Nat Neurosci* **1**(8): 659-667.

Nayak TK, Vij R, Bruhova I, Shandilya J and Auerbach A (2019) Efficiency measures the conversion of agonist binding energy into receptor conformational change. *J Gen Physiol* **151**(4): 465-477.

Nicoll RA and Schulman H (2023) Synaptic memory and CaMKII. *Physiol Rev* **103**(4): 2877-2925.

Paton WD and Rang HP (1966) A kinetic approach to the mechanism of drug action, in *Adv Drug Res* (Harper NJ and Simmonds AB eds) pp 57-80, Academic Press, London

Rauner C and Kohr G (2011) Triheteromeric NR1/NR2A/NR2B receptors constitute the major N-methyl-D-aspartate receptor population in adult hippocampal synapses. *J Biol Chem* **286**(9): 7558-7566.

Riddy DM, Valant C, Rueda P, Charman WN, Sexton PM, Summers RJ, Christopoulos A and Langmead CJ (2015) Label-Free Kinetics: Exploiting Functional Hemi-Equilibrium to Derive Rate Constants for Muscarinic Receptor Antagonists. *Mol Pharmacol* **88**(4): 779-790.

Risgaard R, Nielsen SD, Hansen KB, Jensen CM, Nielsen B, Traynelis SF and Clausen RP (2013) Development of 2'-substituted (2S,1'R,2'S)-2-(carboxycyclopropyl)glycine analogues as potent N-methyl-d-aspartic acid receptor agonists. *J Med Chem* **56**(10): 4071-4081.

Romero-Hernandez A, Simorowski N, Karakas E and Furukawa H (2016) Molecular Basis for Subtype Specificity and High-Affinity Zinc Inhibition in the GluN1-GluN2A NMDA Receptor Amino-Terminal Domain. *Neuron* **92**(6): 1324-1336.

Rouzbeh N, Rau AR, Benton AJ, Yi F, Anderson CM, Johns MR, Jensen L, Lotti JS, Holley DC and Hansen KB (2023) Allosteric modulation of GluN1/GluN3 NMDA receptors by GluN1-selective competitive antagonists. *J Gen Physiol* **155**(6).

Schorge S, Elenes S and Colquhoun D (2005) Maximum likelihood fitting of single channel NMDA activity with a mechanism composed of independent dimers of subunits. *J Physiol* **569**(Pt 2): 395-418.

Stroebel D, Casado M and Paoletti P (2018) Triheteromeric NMDA receptors: from structure to

synaptic physiology. *Curr Opin Physiol* **2**: 1-12.

Sun W, Hansen KB and Jahr CE (2017) Allosteric Interactions between NMDA Receptor Subunits Shape the Developmental Shift in Channel Properties. *Neuron* **94**(1): 58-64 e53.

Vance KM, Simorowski N, Traynelis SF and Furukawa H (2011) Ligand-specific deactivation time course of GluN1/GluN2D NMDA receptors. *Nat Commun* **2**: 294.

Vicini S, Wang JF, Li JH, Zhu WJ, Wang YH, Luo JH, Wolfe BB and Grayson DR (1998) Functional and pharmacological differences between recombinant N-methyl-D-aspartate receptors. *J Neurophysiol* **79**(2): 555-566.

Volkmann RA, Fanger CM, Anderson DR, Sirivolu VR, Paschetto K, Gordon E, Virginio C, Gleyzes M, Buisson B, Steidl E, Mierau SB, Fagiolini M and Menniti FS (2016) MPX-004 and MPX-007: New Pharmacological Tools to Study the Physiology of NMDA Receptors Containing the GluN2A Subunit. *PLoS ONE* **11**(2): e0148129.

Wang H, Lv S, Stroebel D, Zhang J, Pan Y, Huang X, Zhang X, Paoletti P and Zhu S (2021) Gating mechanism and a modulatory niche of human GluN1-GluN2A NMDA receptors. *Neuron* **109**(15): 2443-2456 e2445.

Williams K (1993) Ifenprodil discriminates subtypes of the N-methyl-D-aspartate receptor: selectivity and mechanisms at recombinant heteromeric receptors. *Mol Pharmacol* **44**(4): 851-859.

Wu E, Zhang J, Zhang J and Zhu S (2023) Structural insights into gating mechanism and allosteric regulation of NMDA receptors. *Curr Opin Neurobiol* **83**: 102806.

Yi F, Bhattacharya S, Thompson CM, Traynelis SF and Hansen KB (2019) Functional and pharmacological properties of triheteromeric GluN1/2B/2D NMDA receptors. *J Physiol* **597**(22): 5495-5514.

Yi F, Mou TC, Dorsett KN, Volkmann RA, Menniti FS, Sprang SR and Hansen KB (2016) Structural Basis for Negative Allosteric Modulation of GluN2A-Containing NMDA Receptors. *Neuron* **91**(6): 1316-1329.

Yi F, Traynelis SF and Hansen KB (2017) Selective Cell-Surface Expression of Triheteromeric NMDA Receptors. *Methods Mol Biol* **1677**: 145-162.

Yi F, Zachariassen LG, Dorsett KN and Hansen KB (2018) Properties of Triheteromeric N-Methyl-d-Aspartate Receptors Containing Two Distinct GluN1 Isoforms. *Mol Pharmacol* **93**(5): 453-467.

Yuan H, Erreger K, Dravid SM and Traynelis SF (2005) Conserved structural and functional control of N-methyl-D-aspartate receptor gating by transmembrane domain M3. *J Biol Chem* **280**(33): 29708-29716.

Yuan H, Hansen KB, Vance KM, Ogden KK and Traynelis SF (2009) Control of NMDA receptor function by the NR2 subunit amino-terminal domain. *J Neurosci* **29**(39): 12045-12058.

Zhao F, Atxabal U, Mariottini S, Yi F, Lotti JS, Rouzbeh N, Liu N, Bunch L, Hansen KB and Clausen RP (2022) Derivatives of (R)-3-(5-Furanyl)carboxamido-2-aminopropanoic Acid as Potent NMDA Receptor Glycine Site Agonists with GluN2 Subunit-Specific Activity. *J Med Chem* **65**(1): 734-746.

MOLPHARM-AR-2024-000975

Footnotes

This work was supported by the National Institutes of Health [Grants P30GM140963, R01NS097536]. No author has an actual or perceived conflict of interest with the contents of this article.

Molecular Pharmacology Fast Forward. Published on November 5, 2024 as DOI: 10.1124/molpharm.124.000975
This article has not been copyedited and formatted. The final version may differ from this version.

Figure legends

Figure 1. Pharmacological equilibrium model for activation and allosteric modulation of NMDA receptors. (A) Surface representation of the GluN1/2A NMDA receptor structure (PDB ID 7EOS; (Wang et al., 2021). (B) Cartoon representation of N-terminal domains (NTDs), agonist binding domains (ABDs), and the transmembrane domain (TMD) in NMDA receptor structures. Allosteric modulators with known binding sites are indicated in the different layers of the structure. Each modulator has two equivalent binding sites; a single binding site in each of the two GluN1-GluN2 dimers. GluN1 (e.g. glycine) and GluN2 (e.g. glutamate) agonists are depicted as white and orange ovals, respectively. (C) Chemical structures of GluN2A-selective negative allosteric modulators (NAMs). (D) Pharmacological equilibrium model describing binding of an agonist A and activation of the NMDA receptor R using two parameters, namely agonist binding affinity K_a (i.e. the inverse of the agonist binding dissociation constant $K_A = 1/K_a$) and agonist efficacy E. The model also describes the binding affinity of a modulator B and the strength by which this modulator can change agonist binding affinity and efficacy. The allosteric modulation is described using three parameters, namely modulator binding affinity K_b (i.e. $K_B = 1/K_b$), allosteric binding constant α, and allosteric efficacy constant β. NMDA receptors require full agonist occupancy at both coagonist binding sites (e.g. glutamate and glycine) for activation, but the model only considers binding of one coagonist (e.g. glycine) and assumes full occupancy by the other coagonist (e.g. glutamate). (E) Illustration of agonist binding to receptors with only a single modulator bound to an allosteric binding site at the interface between GluN1 and GluN2 subunits. The agonist can bind first to the modulator-lacking GluN1-GluN2 dimer (ARB) or bind first to the dimer with bound modulator (ABR). (F) Agonist concentration-response data in the

Molecular Pharmacology Fast Forward. Published on November 5, 2024 as DOI: 10.1124/molpharm.124.000975
This article has not been copyedited and formatted. The final version may differ from this version.

absence and presence of increasing NAM concentrations simulated using Equation 1, which is derived from the equilibrium model (see Materials and Methods; see also Supplemental Information for the derivation of the equation). The data are normalized to the maximal agonist response in the absence of modulator. Agonist efficacy (E = 0.5), agonist binding dissociation constant (K_A = 0.5 μM), and modulator binding dissociation constant (K_B = 0.5 μM) were kept constant in the simulations, but allosteric binding constant α and allosteric efficacy constant β were varied.

Figure 2. Determination of agonist binding affinity and agonist efficacy. (A) Chemical structures of NMDA receptor agonists that bind the glycine site (AICP, UCM-F-8d, and glycine) or the glutamate site (glutamate, NMDA, and Me-CCG). (B) Representative two-electrode voltage-clamp recordings of responses from GluN1-A652C/2A receptors activated by saturating agonist concentrations. Responses to glycine, AICP, and UCM-F-8d were activated in the presence of 300 μM glutamate and responses to NMDA and Me-CCG were activated in the presence of 100 μM glycine. Responses in the presence of agonist ($I_{agonist}$) correspond to maximal P_{open} for the respective coagonist pair, while MTSEA-modification locks the channel in an open conformation with $P_{open} \approx 1$ (I_{MTSEA}). (C) Bar graph summarizing maximal P_{open} for the coagonist pairs. Maximal P_{open} values were calculated from $I_{agonist}/I_{MTSEA}$ as described in Materials and Methods. Data are shown as mean ± SD from 15-36 oocytes. (D) Representative two-electrode voltage-clamp recordings of concentration-response data for glycine and glutamate at GluN1/2A receptors. (E-F) Concentration-response data for glycine site agonists (E) and glutamate site agonists (F) in the presence of 300μM glutamate or 100 μM glycine, respectively. Agonist

Molecular Pharmacology Fast Forward. Published on November 5, 2024 as DOI: 10.1124/molpharm.124.000975
This article has not been copyedited and formatted. The final version may differ from this version.

binding dissociation constants K_A were determined by fitting Equation 7 to the concentration-response data with agonist efficacy E fixed to the values from Table 1 (errors for fixed values were not included in the analyses). Data are shown as mean ± SD from 14-28 oocytes. See Table 1 for fitted parameters and additional details.

Figure 3. Challenges related to achieving agonist/modulator/receptor equilibrium for GluN2A-selective NAMs. (A) Representative two-electrode voltage-clamp recordings of responses from GluN1/2A receptors activated by 10 μM glycine in the presence of 300 μM glutamate and vehicle (0.1% DMSO) or 0.3 μM MPX-007. Steady-state responses (i.e. equilibrium indicated at 100%) are achieved relatively quickly in vehicle compared to in the presence of MPX-007. (B) Bar graph summarizing the short glycine exposure needed to achieve equilibrium in vehicle compared to the prolonged exposure to glycine required to reach equilibrium in MPX-007. Responses are measured at different time points following glycine exposure and are normalized to the time point indicated by 100% in (A). Data are shown as mean ± SD from 6 oocytes. (C) Representative two-electrode voltage-clamp recordings of responses from GluN1/2A receptors activated by different glycine concentrations in the presence of 300 μM glutamate and in the absence or presence of vehicle (0.1% DMSO) or 0.1 μM NAM. Steady-state responses are measured in vehicle and TCN-201, whereas equilibrium is not observed in MPX-004 or MPX-007. Thus, prolonged (>> 5 min) measurements for each glycine concentration would be required to achieve steady-state responses in 0.1 μM MPX-004 or MPX-007, which is not practically feasible. (D) Glycine concentration-response data measured in vehicle or in the presence of 0.1 μM NAM. The shallow Hill slopes of concentration-response data measured in MPX-004 or MPX-007 indicate non-equilibrium conditions as illustrated in (C). Data are normalized to

Molecular Pharmacology Fast Forward. Published on November 5, 2024 as DOI: 10.1124/molpharm.124.000975
This article has not been copyedited and formatted. The final version may differ from this version.

control responses measured in the absence of vehicle or NAM.

Figure 4. Determination of allosteric efficacy constant β at hemi-equilibrium. (A) Representative whole-cell patch-clamp recordings of responses from GluN1/2A receptors expressed in HEK293T cells. Maximal responses are activated by 30 mM glycine during the time indicated by the black bar above the recording in the continuous presence of 300 μM glutamate and vehicle (0.01-0.03% DMSO), 10 μM MPX-004, 10 μM MPX-007, or 3 μM TCN-201. The slow NAM unbinding rate enables determination of the allosteric efficacy constant β at hemi-equilibrium when GluN1/2A receptors are fully bound by NAM and maximally activated by glycine. Asterisks indicate current responses caused by artifacts related to the perfusion system and solution exchange. (B) Expanded view of the glycine-activated current response in the presence of 3 μM TCN-201. In the presence of TCN-201, the initial response amplitude is smaller than responses from glycine alone due to a reduction in glycine agonist efficacy mediated by TCN-201 binding. However, the current amplitude increases with TCN-201 unbinding as agonist efficacy is no longer reduced. The TCN-201 unbinding time course was fitted with a mono-exponential function to produce a time constant of 230 ± 100 ms (N = 6). (C) Bar graph summarizing effects of vehicle or NAM on maximal glycine responses. Data are shown as mean ± SD from 8-19 oocytes. All data are significantly different from each other ($p < 0.05$; # indicates significantly different from vehicle), except for TCN-201 compared to MPX-007 ($p > 0.05$; one-way ANOVA with Tukey-Kramer multiple comparisons). See Table 2 for allosteric efficacy constants β calculated from $I_{NAM}/I_{control}$.

Figure 5. Modulation of glutamate potency and agonist efficacy by GluN2A-selective NAMs.

Molecular Pharmacology Fast Forward. Published on November 5, 2024 as DOI: 10.1124/molpharm.124.000975
This article has not been copyedited and formatted. The final version may differ from this version.

(A) Engineered disulfide bonds are introduced by N499C+Q686C mutations in each of the GluN1 subunits (GluN1-CC). The disulfide bonds restrict the GluN1 agonist binding domain in a closed conformation, which mimics the glycine bound state and enables receptor activation by glutamate alone. (B) Representative two-electrode voltage-clamp recordings of responses from GluN1-CC/2A receptors activated by glutamate in the presence of vehicle (0.1% DMSO) or 10 μM MPX-004. (C-E) Concentration-response data for glutamate in the presence (C) 5 μM TCN-201, (D) 10 μM MPX-004, or (E) 10 μM MPX-007 and vehicle (0.05%, 0.1%, and 0.03% DMSO, respectively). Responses are normalized to the control response in the absence of vehicle or NAM. Data are shown as mean ± SD from 7-21 oocytes. * indicates that the fitted maximal responses are significantly different ($p < 0.05$; one-way ANOVA with Tukey-Kramer multiple comparisons). See Table 3 for EC_{50} values and maximal responses, as well as statistical tests.

Figure 6. Determination of allosteric binding constant α at hemi-equilibrium. (A) Representative whole-cell patch-clamp recordings of responses from GluN1/2A receptors to increasing concentrations of glycine in the continuous presence of 300 μM glutamate and 10 μM MPX-004. Responses are normalized to the maximal response to 10 mM glycine and overlaid. The slow NAM unbinding rate enables determination of glycine concentration-response data at hemi-equilibrium before appreciable NAM unbinding occurs. (B) Glycine concentration response data measured at hemi-equilibrium in vehicle (0.1% DMSO) and following pre-exposure to 10 μM MPX-004 or 10 μM MPX-007. Agonist binding affinity K_a and allosteric binding constants α are determined by fitting Equation 9 to the data with fixed agonist efficacy E = 0.66 and values of allosteric efficacy constants β for MPX-004 and MPX-007 from Table 2 (errors for fixed values

Molecular Pharmacology Fast Forward. Published on November 5, 2024 as DOI: 10.1124/molpharm.124.000975
This article has not been copyedited and formatted. The final version may differ from this version.

were not included in the analyses). Data are shown as mean ± SD from 8-9 cells. (C) Representative whole-cell patch-clamp recordings of responses from GluN1/2A receptors to increasing concentrations of glycine in the continuous presence of 300 µM glutamate and 3 µM TCN-201. Glycine exposure was limited to 15 ms due to the faster unbinding of TCN-201 in the presence of glycine compared to MPX-004 and MPX-007. (D) Glycine concentration response data at hemi-equilibrium in vehicle (0.03% DMSO) and following pre-exposure to 3 µM TCN-201. Agonist binding affinity K_a and allosteric binding constants α are determined by fitting Equation 9 to the data with fixed agonist efficacy E = 0.66 and allosteric efficacy constant β for TCN-201 from Table 2 (errors for fixed values were not included in the analyses). Data are shown as mean ± SD from 7-8 cells. See Tables 1 and 2 for parameters determined by fitting with Equation 9.

Figure 7. Determination of modulator binding dissociation constant K_B at equilibrium. (A) Representative two-electrode voltage-clamp recordings of glycine concentration-response data at GluN1/2A receptors in the presence 300 µM glutamate and of high NAM concentrations. (B) Glycine concentration-response data measured in vehicle (0.01-0.05% DMSO) and the presence of intermediate to high NAM concentrations, at which equilibrium could be reached in a reasonable time. The data are normalized to the initial control response to saturating glycine before exposure to vehicle or NAM and modulator binding dissociation constants K_B are determined by fitting Equation 8 to the data with K_A, E, α, and β fixed to the values listed in Tables 1 and 2 (errors for fixed values were not included in the analyses). Normalized minimum and maximum responses (I_{min} and I_{max}, respectively) were variables in the global non-linear regression fitting and allowed to vary for each NAM concentration. Data are shown as mean ±

Molecular Pharmacology Fast Forward. Published on November 5, 2024 as DOI: 10.1124/molpharm.124.000975
This article has not been copyedited and formatted. The final version may differ from this version.

SD from 34-75 oocytes. See Table 2 for modulator binding dissociation constants K_B. (C) The sum of squared errors (SSE) calculated as a function of the binding dissociation constant K_B from the fit of Equation 8 with fixed K_a, E, α, and β to the glycine concentration-response data shown in (B).

Figure 8. Allosteric modulation of triheteromeric GluN1/2A/2B receptors. (A) Representative two-electrode voltage-clamp recordings of responses from triheteromeric GluN1-A652C/2A_{C1}/2B_{C2} and diheteromeric GluN1-A652C/2B receptors activated by saturating glycine (100 μM) in the presence of 300 μM glutamate. Responses in the presence of agonist correspond to maximal P_{open} for glutamate/glycine coagonists, while MTSEA-modification locks the channel in an open conformation with $P_{open} \approx 1$. The bar graph summarizes maximal P_{open} for glutamate/glycine. Data for GluN1/2A are also shown in Figure 2. Data are shown as mean ± SD from 16-36 oocytes. (B) Representative whole-cell patch-clamp recordings of responses from triheteromeric GluN1/2A_{C1}/2B_{C2} receptors expressed in HEK293T cells. Maximal responses are activated by 30 mM glycine during the time indicated by the black bar above the recording in the continuous presence of 300 μM glutamate and vehicle (0.03% DMSO) or 3 μM TCN-201. The asterisk indicates a current response caused by artifacts related to the perfusion system and solution exchange. The bar graph summarizes the effects of vehicle or NAM on maximal glycine responses. All data are significantly different from each other ($p < 0.05$; # indicates significantly different from vehicle), except for TCN-201 compared to MPX-007 ($p > 0.05$; one-way ANOVA with Tukey-Kramer multiple comparisons). Data are shown as mean ± SD from 10-12 cells. (C) Representative whole-cell patch-clamp recordings of responses from triheteromeric

Molecular Pharmacology Fast Forward. Published on November 5, 2024 as DOI: 10.1124/molpharm.124.000975
This article has not been copyedited and formatted. The final version may differ from this version.

GluN1/2A_{C1}/2B_{C2} receptors to increasing concentrations of glycine in the continuous presence of 300 µM glutamate and 10 µM MPX-004. Responses are normalized to the maximal response to 10 mM glycine and overlaid. The graph summarizes glycine concentration-response data measured at hemi-equilibrium in vehicle (0.01% DMSO) and following pre-exposure to 10 µM MPX-004 or 1 µM MPX-007. Agonist binding affinity K_a and allosteric binding constants α are determined by fitting Equation 12 to the data with fixed agonist efficacy E = 0.17 and allosteric efficacy constants β from Table 2 (errors for fixed values were not included in the analyses). Data are shown as mean ± SD from 9-13 cells. (D) Representative whole-cell patch-clamp recordings of responses from triheteromeric GluN1/2A_{C1}/2B_{C2} receptors to increasing concentrations of glycine in the continuous presence of 300 µM glutamate and 3 µM TCN-201. Glycine exposure was limited to 20 ms due to faster unbinding of TCN-201 in the presence of glycine compared to MPX-004 and MPX-007. The graph summarizes glycine concentration-response data at hemi-equilibrium in vehicle (0.03% DMSO) and following pre-exposure to 3 µM TCN-201. Data are shown as mean ± SD from 9-11 cells. See Tables 1 and 2 for fitted parameters for triheteromeric GluN1/2A/2B receptors.

Figure 9. Allosteric modulation by GluN2A-selective antagonists. (A) Glycine concentration-response data for GluN1/2A receptors in the absence and presence of GluN2A-selective NAMs simulated using Equation 8 and experimentally determined parameters listed in Tables 1 and 2. (B-C) Simulations of NAM concentration-inhibition data for diheteromeric GluN1/2A and triheteromeric GluN1/2A/2B receptors activated by increasing glycine concentrations. Red dashed lines indicate NAM solubility limits (8 µM, 16 µM, and 68 µM for TCN-201, MPX-004, and MPX-007, respectively; (Volkmann et al., 2016).

Molecular Pharmacology Fast Forward. Published on November 5, 2024 as DOI: 10.1124/molpharm.124.000975
This article has not been copyedited and formatted. The final version may differ from this version.

Table 1. Parameters describing agonist activity at NMDA receptors.

Receptor subtype	Agonists	Maximal P_{open} (95% CI)	E (95% CI)	N	K_A (μM) (95% CI)	EC_{50} (μM) (95% CI)	n_H	N
GluN1/2A	glycine [a]	0.39 (0.38 - 0.41)	0.66 (0.61 - 0.70)	36	0.66 [b] (0.60 - 0.72)	1.03 [b] (0.94 - 1.13)	1.6	28
	glycine [a]	-	-	-	0.93 [c] (0.81 - 1.07)	1.43 [c] (1.25 - 1.64)	1.6	9
	UCM-F-8d [a]	0.044 (0.041 - 0.048)	0.046 (0.043 - 0.05)	15	0.033 [b] (0.031 - 0.035)	0.082 [b] (0.076 - 0.088)	1.4	18
	AICP [a]	0.36 (0.35 - 0.38)	0.57 (0.53 - 0.61)	24	0.041 [b] (0.037 - 0.046)	0.064 [b] (0.057 - 0.072)	1.5	14
	glutamate [d,e]	0.39 (0.38 - 0.41)	0.66 (0.61 - 0.70)	36	2.21 [b] (1.96 - 2.48)	3.45 [b] (3.05 - 3.90)	1.4	28
	NMDA [d]	0.29 (0.28 - 0.30)	0.41 (0.39 - 0.44)	23	50 [b] (48 - 53)	88 [b] (82 - 94)	1.3	14
	Me-CCG [d]	0.29 (0.28 - 0.31)	0.42 (0.39 - 0.45)	15	0.11 [b] (0.10 - 0.13)	0.21 [b] (0.19 - 0.24)	1.4	16
GluN1/2A$_{C1}$/2B$_{C2}$	glycine [a]	0.15 (0.13 - 0.16)	0.17 (0.16 - 0.19)	26	0.48 [c] (0.41 - 0.57)	0.99 [c] (0.83 - 1.18)	1.6	9
GluN1/2B	glycine [a]	0.026 (0.021 - 0.031)	0.026 (0.022 - 0.032)	16	0.27 [c] (0.23 - 0.31)	0.60 [c] (0.52 - 0.70)	1.3	7

Estimated maximal open probability (P_{open}) was determined using a modified soluble cysteine accessibility method for GluN1-A652C/2A, GluN1-A652C/2A$_{C1}$/2B$_{C2}$, and GluN1-A652C/2B receptors activated by a saturating concentration of the indicated agonist in the presence of saturating co-agonist (glutamate or glycine). Agonist efficacy E was calculated from maximal P_{open} using Equation 5. The agonist binding dissociation constant K_A was determined by fitting Equation 7 with fixed E to concentration-response data for the indicated agonist. Agonist potency EC_{50} and Hill slope (n_H) were determined by fitting the concentration-response data to the Hill equation. Data are shown with asymmetric 95% confidence intervals (95% CIs). - indicates same as values above. N is the number of oocytes used as experimental sample size. See Supplemental Table S1 for logarithmic mean ± SD values used to calculate 95% CIs.

Molecular Pharmacology Fast Forward. Published on November 5, 2024 as DOI: 10.1124/molpharm.124.000975
This article has not been copyedited and formatted. The final version may differ from this version.

[a] Determined in the presence of 300 µM glutamate.

[b] Concentration-response data determined using two-electrode voltage-clamp recordings.

[c] Concentration-response data determined using whole-cell patch-clamp recordings.

[d] Determined in the presence of 100 µM glycine.

[e] Maximal P_{open} values for glutamate and glycine were determined in the same experiment.

Molecular Pharmacology Fast Forward. Published on November 5, 2024 as DOI: 10.1124/molpharm.124.000975
This article has not been copyedited and formatted. The final version may differ from this version.

Table 2. Parameters describing allosteric modulation of GluN2A-containing NMDA receptors.

Receptor subtype	Modulator	K_B (nM) (95% CI)	N	α (95% CI)	N	β (95% CI)	N
GluN1/2A	TCN-201	42 (39 – 46)	75	0.0032 $^{\#}$ (0.0021 - 0.0048)	7	0.76 (0.71 - 0.80)	10
	MPX-004	9.3 (7.8 – 11.1)	34	0.0018 $^{*,\#}$ (0.0015 - 0.0022)	8	1.2 $^{*,\#}$ (1.1 - 1.3)	10
	MPX-007	1.1 (0.9 – 1.3)	40	0.00053 * (0.00046 - 0.00060)	9	0.82 (0.75 - 0.90)	8
GluN1/2A$_{C1}$/2B$_{C2}$	TCN-201	ND [a]		0.0068 $^{\#,ns}$ (0.0039 - 0.012)	11	0.75 ^{ns} (0.64 - 0.88)	11
	MPX-004	ND [a]		0.0021 $^{*,\#,ns}$ (0.0012 - 0.0037)	13	1.3 $^{*,\#,ns}$ (1.2 - 1.4)	10
	MPX-007	ND [a]		0.00074 ^{*,ns} (0.00061 - 0.00090)	9	0.84 ^{ns} (0.76 - 0.92)	12

Modulator binding dissociation constants K_B were determined by fitting Equation 8 with fixed K_A, E, α and β to glycine concentration-response data measured using two-electrode voltage-clamp recordings in the absence and presence of different NAM concentrations. K_B values are shown with asymmetric 95% confidence intervals (95% CIs) taken directly from the best global nonlinear regression fit to all the data. Allosteric binding constants α and allosteric efficacy constants β were determined at hemi-equilibrium using whole-cell patch-clamp recordings in the absence and presence of NAM. Data are shown with asymmetric 95% CIs and N is the number of oocytes or HEK293T cells used as experimental sample size. * indicates significantly different from TCN-201 and $^{\#}$ indicates significantly different from MPX-007 for the same receptor subtype ($p < 0.05$; two-way ANOVA with Tukey-Kramer multiple comparisons). ^{ns} indicates no significant difference from GluN1/2A for the same NAM ($p > 0.05$; two-way ANOVA with Tukey-Kramer multiple comparisons). Statistical tests were performed using log(α) and log(β) values (Christopoulos, 1998). See Supplemental Table S2 for logarithmic mean ± SD values used

Molecular Pharmacology Fast Forward. Published on November 5, 2024 as DOI: 10.1124/molpharm.124.000975
This article has not been copyedited and formatted. The final version may differ from this version.

to calculate 95% CIs.

[a] Binding dissociation constants K_B are assumed to be conserved between GluN1/2A and GluN1/2A_{C1}/2B_{C2}.

Molecular Pharmacology Fast Forward. Published on November 5, 2024 as DOI: 10.1124/molpharm.124.000975
This article has not been copyedited and formatted. The final version may differ from this version.

Table 3. Modulation of crosslinked GluN1-CC/2A receptors by GluN2A-selective NAMs.

Modulator	EC_{50} (μM) (95% CI)	n_H	I_{max} (mean ± SD)	Relative I_{max} (% of vehicle)	N
vehicle	2.1 (1.7 - 2.6)	1.6	88 ± 10	100	21
TCN-201	2.5 (1.7 - 3.8)	1.5	91 ± 9	103	7
MPX-004	1.1 * (0.9 - 1.3)	1.4	110 ± 10 *	118 *	8
MPX-007	1.3 * (1.0 - 1.7)	1.5	87 ± 11	99	7

Concentration-response data for glutamate activation of GluN1-CC/2A receptors measured in the absence (vehicle; 0.05 - 0.1% DMSO) or presence of 5 μM TCN-201, 10 μM MPX-004, or 10 μM MPX-007 using two-electrode voltage-clamp recordings. Engineered disulfide bonds are introduced by N499C+Q686C mutations in each of the GluN1 subunits (GluN1-CC) to restrict the GluN1 agonist binding domain in a closed conformation, which mimics the glycine bound state and enables receptor activation by glutamate alone. I_{max} is the fitted maximal glutamate response normalized to a maximal glutamate response at the beginning of the recording before vehicle or NAM exposure. The vehicle control reveals that the response amplitudes are slightly reduced over the duration of the recordings. Data are shown with asymmetric 95% confidence intervals (95% CIs) or as mean ± SD. N is the number of oocytes used as experimental sample size. * indicates significantly different from vehicle ($p < 0.05$; one-way ANOVA with Tukey-Kramer multiple comparisons). Statistical test were performed using log(EC_{50}) values (Christopoulos, 1998). See Supplemental Table S3 for logarithmic mean ± SD values used to calculate 95% CIs.

Figure 1

Molecular Pharmacology Fast Forward. Published on November 5, 2024 as DOI: 10.1124/molpharm.124.000975
This article has not been copyedited and formatted. The final version may differ from this version.

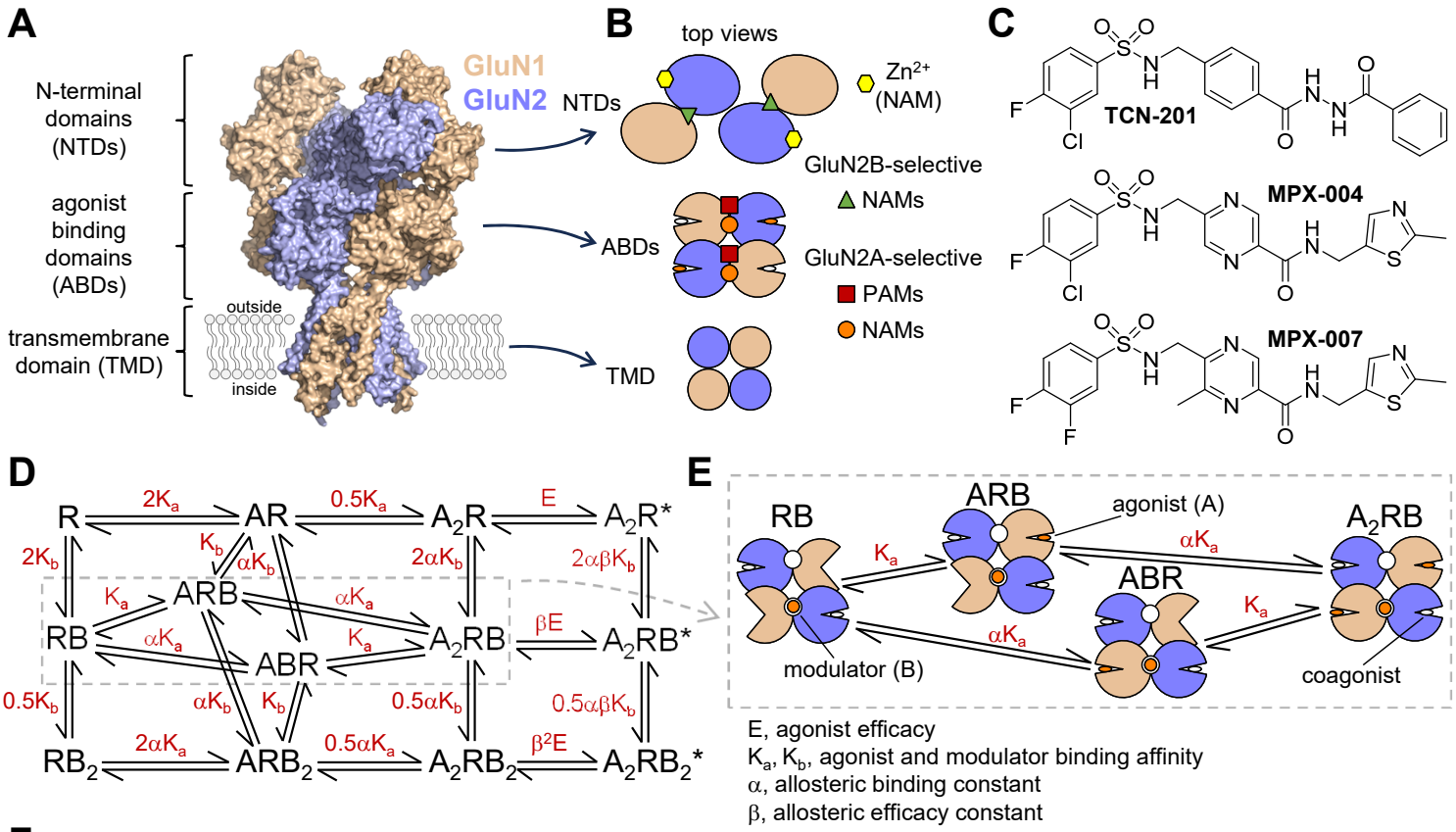

Molecular Pharmacology Fast Forward. Published on November 5, 2024 as DOI: 10.1124/molpharm.124.000975
This article has not been copyedited and formatted. The final version may differ from this version.

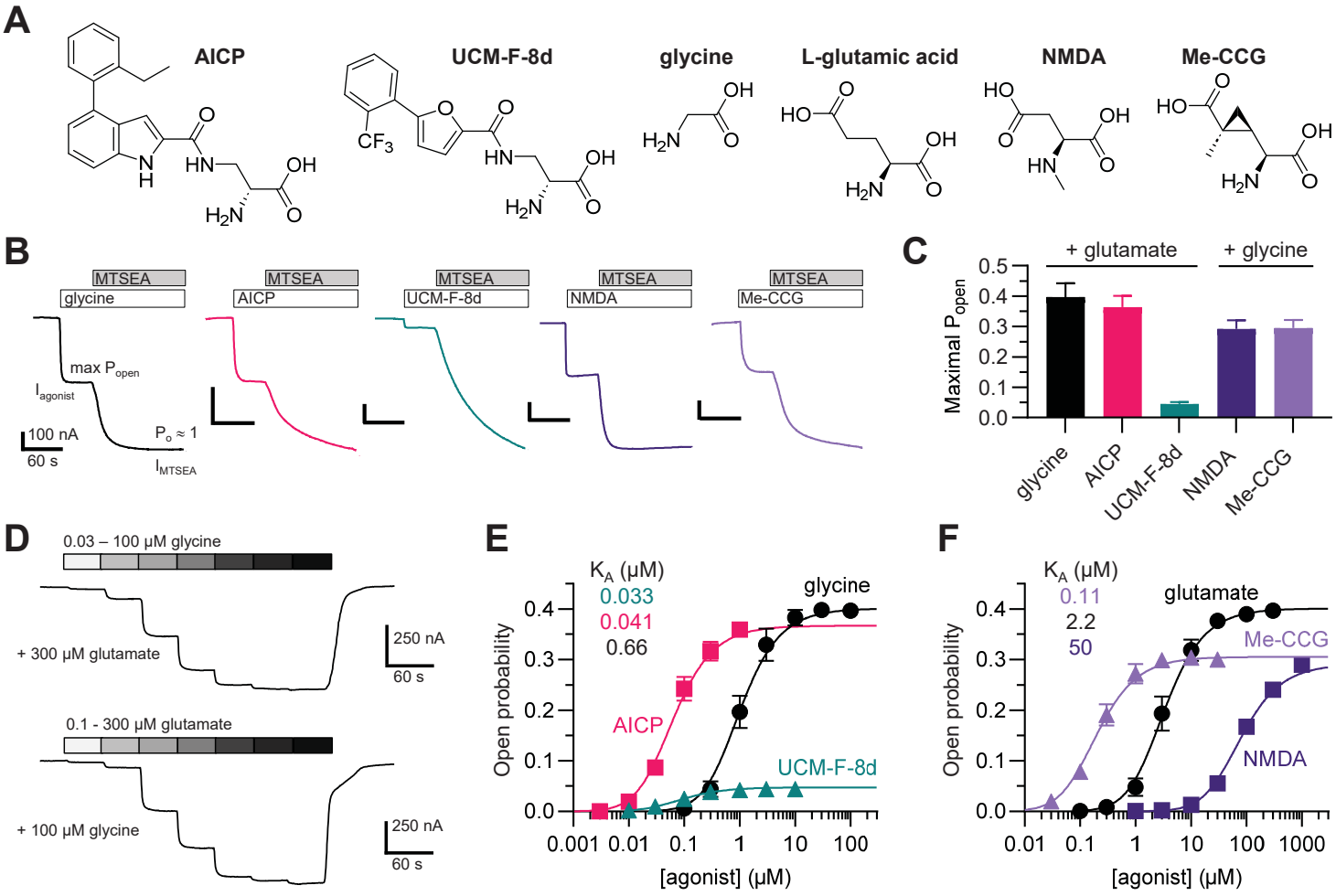

Figure 3

Molecular Pharmacology Fast Forward. Published on November 5, 2024 as DOI: 10.1124/molpharm.124.000975
This article has not been copyedited and formatted. The final version may differ from this version.

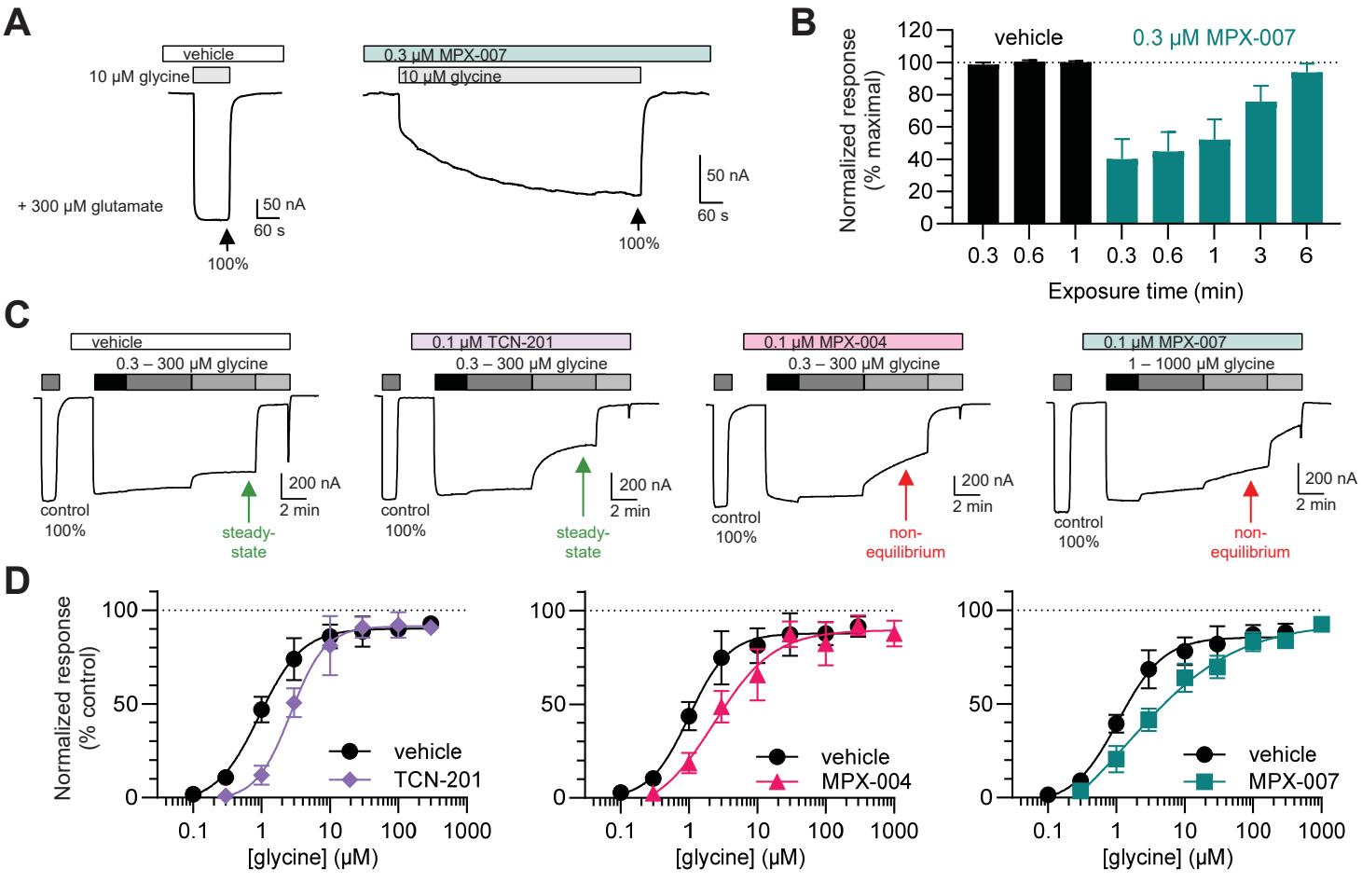

Figure 4

Molecular Pharmacology Fast Forward. Published on November 5, 2024 as DOI: 10.1124/molpharm.124.000975
This article has not been copyedited and formatted. The final version may differ from this version.

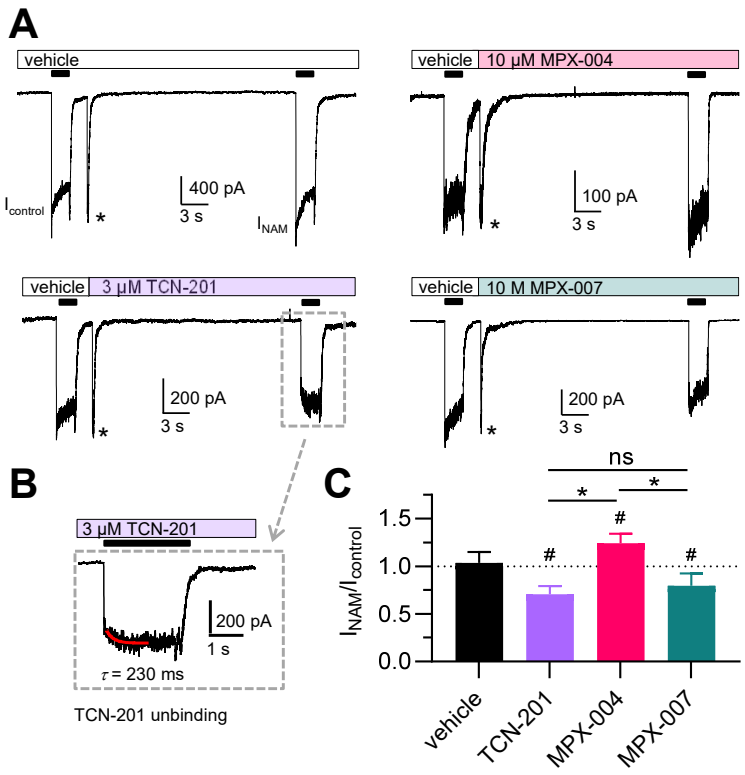

Figure 5

Molecular Pharmacology Fast Forward. Published on November 5, 2024 as DOI: 10.1124/molpharm.124.000975
This article has not been copyedited and formatted. The final version may differ from this version.

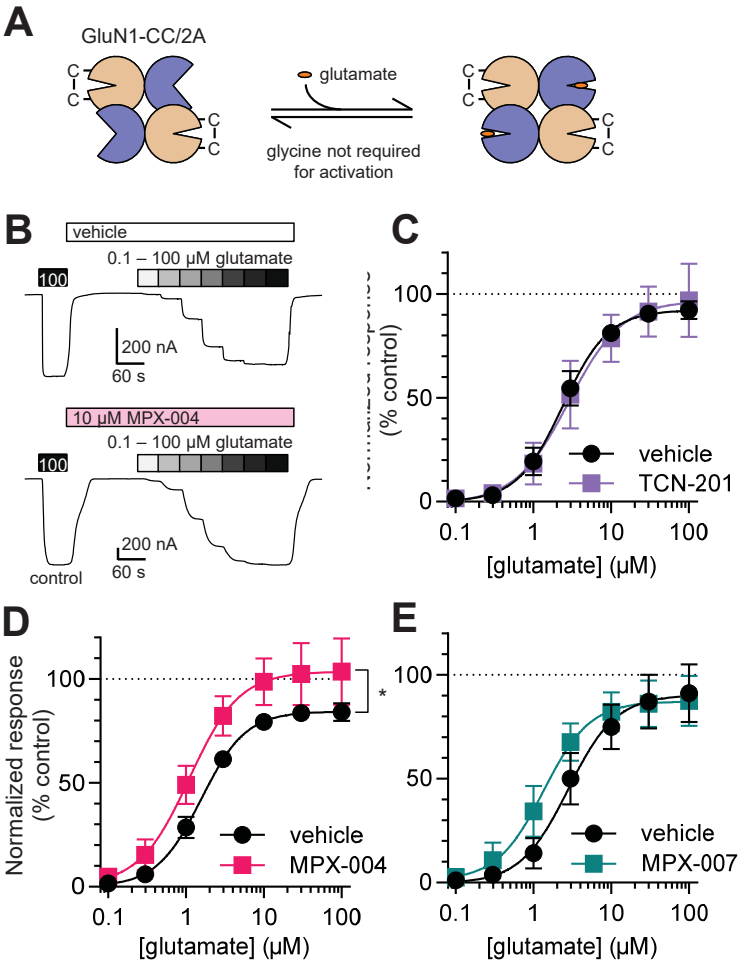

Molecular Pharmacology Fast Forward. Published on November 5, 2024 as DOI: 10.1124/molpharm.124.000975
This article has not been copyedited and formatted. The final version may differ from this version.

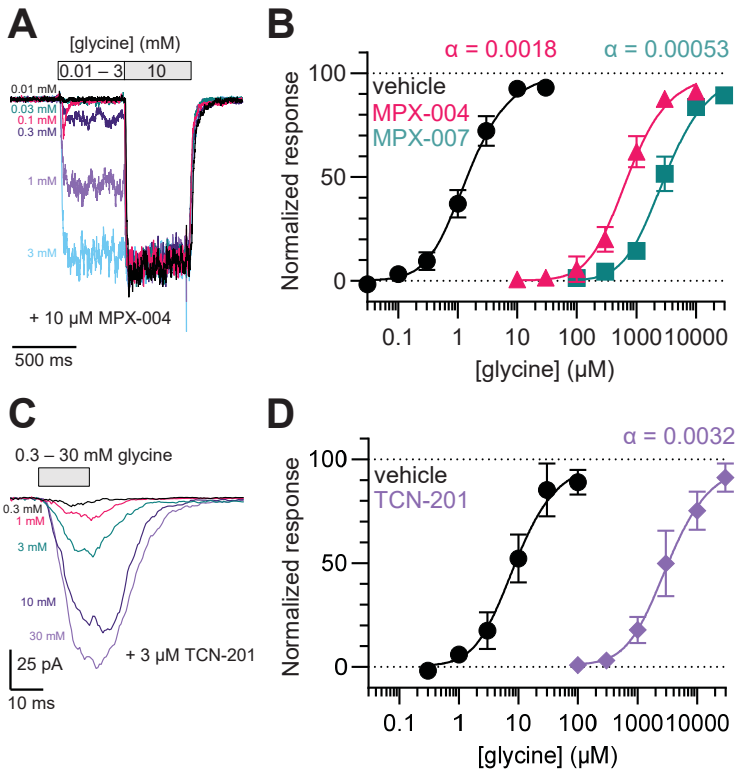

Figure 7

Molecular Pharmacology Fast Forward. Published on November 5, 2024 as DOI: 10.1124/molpharm.124.000975
This article has not been copyedited and formatted. The final version may differ from this version.

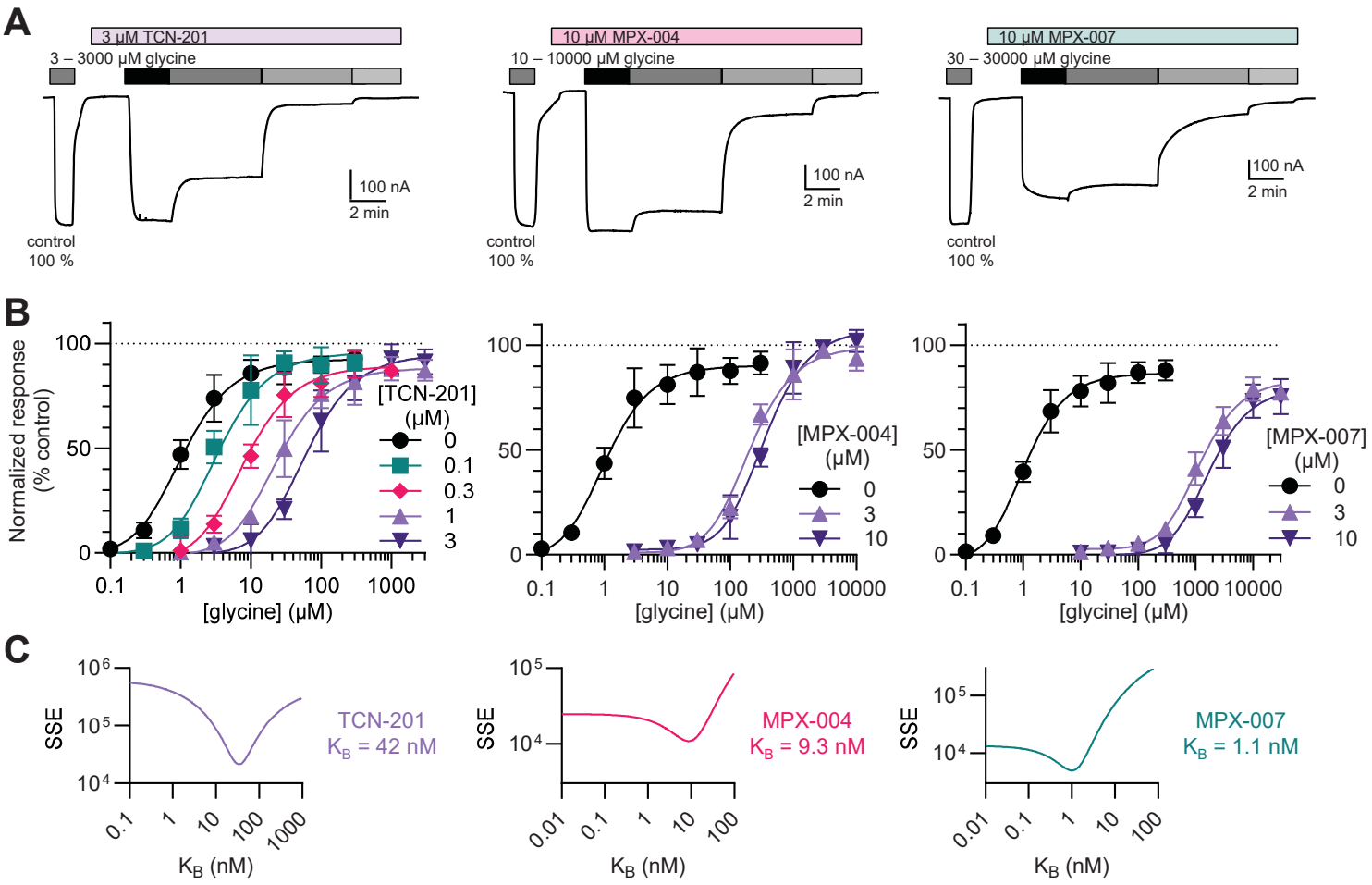

Figure 8

Molecular Pharmacology Fast Forward. Published on November 5, 2024 as DOI: 10.1124/molpharm.124.000975
This article has not been copyedited and formatted. The final version may differ from this version.

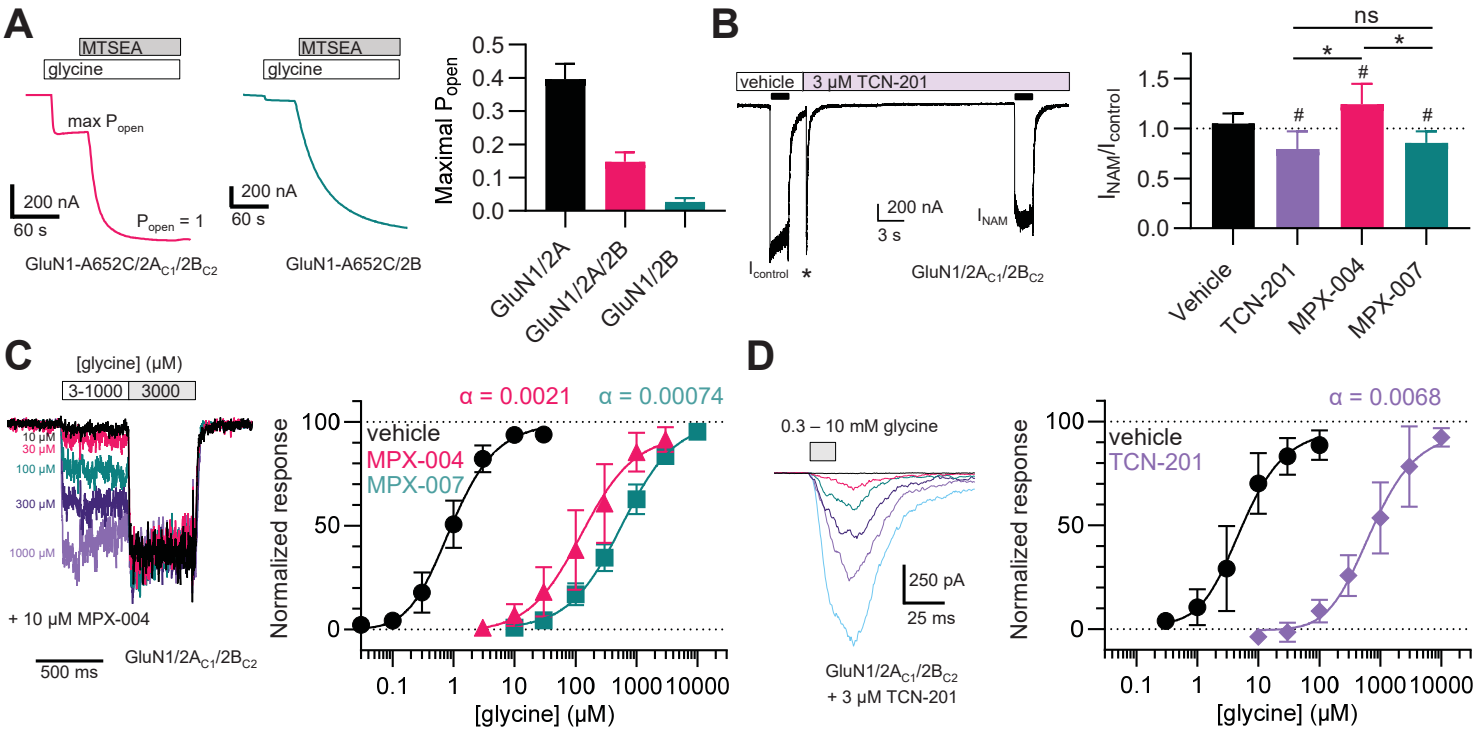

Figure 9

Molecular Pharmacology Fast Forward. Published on November 5, 2024 as DOI: 10.1124/molpharm.124.000975
This article has not been copyedited and formatted. The final version may differ from this version.